Application of Fourier Transform Electron Paramagnetic Resonance in the Study of Photochemical Reactions

Hans van Willigen,* Patricia R. Levstein,† and Marie H. Ebersole‡

Department of Chemistry, University of Massachusetts at Boston, Boston, Massachusetts 02125

Received June 19, 1992 (Revised Manuscript Received October 2, 1992)

Contents

1. Introduction 173
2. Instrumental Aspects 175
3. CIDEP Mechanisms 178
3.1. Triplet Mechanism 178
3.2. Radical Pair Mechanism 179
3.3. Spin-Correlated Radical Pairs 180
3.4. Polarization from Doublet–Quartet Mixing 181
4. Applications 181
4.1. Photoinduced Electron Transfer 181
4.1.1. FT EPR Studies of Porphyrin/Quinone in Homogeneous Solution 181
4.1.2. FT EPR Study of Porphyrin/Quinone in Heterogeneous Media 185
4.2. Acetone Ketyl Radical 189
4.2.1. Background 189
4.2.2. FT EPR Study of Acetone/2-Propanol 190
4.2.3. FT EPR Study of *tert*-Butyl Peroxide/2-Propanol 193
4.2.4. Conclusions 195
5. Concluding Remarks 195

1. Introduction

Early on in the development of EPR, it was recognized that the technique might prove of great value in investigations of the mechanisms and kinetics of chemical reactions. To quote from a review article by Wertz published in this journal in 1955,[1] "In principle, ESR absorption should be an excellent method for directly measuring concentrations of free radicals in the course of a chemical reaction."

The value of EPR in this area of research is due to the following:

(1) Of the reactants, intermediates, and products present in a solution, only those species that carry unpaired electrons can contribute to the spectrum. Hence, one expects spectra to be relatively simple. If the time development of the signal can be measured, it should then be straightforward to determine rate constants.

(2) In general, EPR spectra of free radicals in fluid solution are characterized by high spectral resolution. Information on electron spin–nuclear spin hyperfine interactions and g values derived from the spectra in many cases provides unequivocal evidence for the identity of paramagnetic molecules.[2]

(3) Populations of electron spin states of free radicals formed in chemical reactions initially will deviate from a Boltzmann distribution. This chemically induced dynamic electron polarization (CIDEP) effect, under proper conditions, can manifest itself in the form of enhanced absorption and/or stimulated emission peaks in the EPR spectra. A number of reviews of CIDEP theory and applications have been published in recent years.[3-6] They show that studies of CIDEP effects can provide unique insights into the mechanisms of chemical reactions.

A notable example of the value of the technique is its application in the study of photosynthesis.[7] The following are just a few early results from a long history of EPR studies of the photosynthetic apparatus in green plants and photosynthetic bacteria: (a) In 1956 Commoner et al.[8] established with EPR that light produces free radicals in in vivo photosynthetic organisms. (b) From g value and line-width data, it was deduced that the EPR signals from various photosynthetic reaction center preparations most probably were due to photooxidized chlorophyll molecules located in the reaction centers.[9] (c) From the difference in line widths of EPR signals from in vivo photosynthetic reaction centers and those from in vitro chlorophyl cation radicals, Norris et al.[10] concluded that the in vivo species must be a chlorophyl dimer cation radical (the *special pair*).

These examples illustrate that major contributions to the understanding of chemical reactions can be made with conventional EPR measurements. (By conventional measurement is meant that a continuous-wave (cw), fixed-frequency, microwave source is used, that the measurement involves application of field modulation and phase-sensitive detection, and that the spectrum is recorded by sweeping the magnetic field.[2]) Even so, with standard equipment it is not possible to fully exploit the capabilities of the technique. This is because of the fact that the detection method severely limits the time resolution of the measurement. Typically, the optimum time response of a commercial spectrometer is ~0.1 ms. With the use of field modulation frequencies higher than the 100 kHz typically found in commercial instruments, the response time can be improved by an order of magnitude or so.[11] Even then it may not suffice to directly monitor the progress of chemical reactions. Moreover, spin–lattice relaxation times of free radicals typically are in the nanosecond-to-microsecond time domain. It is evident, therefore, that conventional cw EPR instruments do not have the response time required for time-domain measurements of the evolution of spin state populations under the influence of CIDEP and spin relaxation.

† Present address: INTEC, Güemes 3450, 3000 Santa Fe, Argentina.
‡ Present address: Freie Universität Berlin, Institut für Experimentalphysik, 1000 Berlin 33, Germany.

0009-2665/93/0793-0173$12.00/0

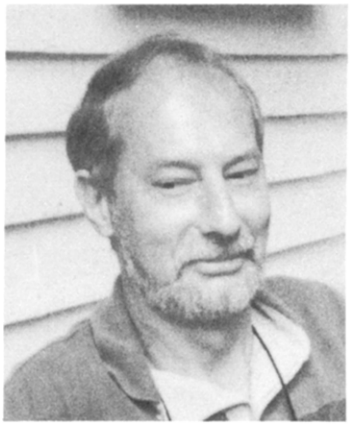

Hans van Willigen was born in Bergen-op-Zoom, The Netherlands, in 1938. He obtained his doctorandus (M.S.) degree, with a major in inorganic chemistry, from the University of Amsterdam in 1963. After performing Ph.D. thesis research under the direction of Prof. S. I. Weissman at Washington University, St. Louis, he was awarded a Ph.D. degree by the University of Amsterdam in 1965. The years from 1965–1969 were spend as wetenschappelijk medewerker in the Laboratory for Molecular Spectroscopy at the University of Nijmegen (The Netherlands). He joined the faculty of the University of Massachusetts at Boston, where he currently holds the position of research professor of chemistry. van Willigen's research deals with the study of the structure and reactivity of paramagnetic systems with EPR and ENDOR techniques. In recent years investigations have focused on the kinetics and mechanisms of photoinduced electron-transfer reactions. He has been visiting professor at the Freie Universität Berlin (Germany) and the University of Jyväskylä (Finland), and was a Fulbright research professor at the Indian Institute of Science in Bangalore.

Patricia R. Levstein was born in Córdoba, Argentina, in 1961. She obtained her master in Biological Chemistry from the National University of Córdoba in 1983. Her Ph.D. thesis research, performed under the direction of Prof. Rafael Calvo, was centered in the application of electron paramagnetic resonance in the study of magneto-structural correlations in metal–amino acid systems. The research was performed at INTEC (Santa Fe, Argentina) and the Ph.D. in Chemistry awarded by the National University of Litoral in 1989. Since then, she worked in applications of the FT EPR technique to photoinduced reactions, as a postdoctoral fellow in Prof. Hans van Willigen's laboratory in the department of Chemistry at the University of Massachusetts at Boston. Since August 1992, she holds a research position of CONICET (Consejo Nacional de Investigaciones Cientificas y Técnicas, Argentina). Her scientific interests comprise experimental and theoretical aspects of electron transfer in biological systems and the correlation with exchange-coupled systems.

Information on chemical kinetics and spin dynamics of photochemical reactions can be obtained indirectly by applying sinusoidal modulation of light intensity combined with phase-sensitive detection of the EPR signal.[12] Amplitude and phase of the signal as functions of light modulation frequency reflects the dynamics of the

Marie H. Ebersole was born in 1952 in Boston, Massachusetts. She obtained a B.A. degree, with a major in English, from the University of Massachusetts at Boston in 1975. After discovering that she really was more interested in the sciences, she enrolled in a graduate program in chemistry. First at the University of Massachusetts/Boston, where she was awarded a M.S. degree, then at the University of Massachusetts/Amherst where she obtained her Ph.D. degree in 1991. Ebersole's thesis research involved the study of photoinduced electron-transfer reactions with the aid of FT EPR and was performed in Boston under direction of Prof. van Willigen. Currently she is a postdoctoral fellow with the group of Prof. Klaus Möbius in the physics department at the Freie Universität Berlin (Germany).

system. The drawback of the method is that data analysis requires a complete understanding of the factors that affect the EPR signal.

The limitations associated with conventional EPR are removed to a large extent with the use of the direct-detection, time-resolved EPR (TREPR) method.[4,6,13,14] In TREPR, the signal is not encoded by application of field modulation. Following the initiation of a chemical reaction with a light pulse or by pulse radiolysis, the time dependence of the signal at a given magnetic field is measured directly using a fast data acquisition system. Alternatively, the spectrum of paramagnetic species present, at a given time after the light or radiolysis pulse, is obtained by sweeping the magnetic field and acquiring the signal with a boxcar integrator. Commercial EPR spectrometers are readily modified so as to make TREPR measurements possible. The time response can be as low as 50 ns.[15]

While TREPR provides excellent time resolution, it has a number of negative characteristics as well. First, the penalty for doing away with phase-sensitive detection is a significant reduction in sensitivity. In most cases the result is that TREPR measurements can cover only the time period during which the spin system is far from thermal equilibrium. Second, the time development of the EPR spectra is governed, in part, by the interaction between spin system and microwave field in the interval between radical formation and signal acquisition. The perturbation will express itself in the form of a strong time dependence of the line width in the time domain where the inverse of the time delay between radical formation and signal detection (τ_d) becomes comparable to or exceeds the intrinsic line width of the EPR signal. With $\tau_d \leq 100$ ns, this means a line-width contribution of a couple of gauss. The off-resonance signal contribution arises because, at the time of detection, the radicals have been exposed to what is in essence a short microwave pulse. It can preclude signal detection or radical identification at

early times ($\tau_d \leq 500$ ns). Apart from affecting line width, the radiation field also influences the time evolution of the signal amplitude.

As a result of these effects, the determination of rate parameters from TREPR spectra must be based on Bloch equations that account not only for chemical kinetics and CIDEP mechanisms but also for the perturbation of the system by the microwave field.[5] The analysis involves a nonlinear, multiparameter, least-squares fit of experimental data to a set of differential equations. The equations must be based on an a priori model that is assumed to account for all processes that play a role in spin state evolution. Because the microwave field may strongly affect the appearance of the EPR spectrum in the early time domain and signals may no longer be detectable as the spin system approaches thermal equilibrium, it can be difficult to assess the validity of the model that is used for the data analysis and the values of the parameters given by the least-squares procedure.

The problems that complicate the analysis of TREPR data can be avoided by application of pulsed-EPR techniques. The objective of time-resolved EPR measurements is to monitor the magnetization along the field direction (z magnetization) associated with the formation and decay of free radicals. This can be accomplished by turning the magnetization vector in the transverse (xy) plane with one or more short microwave pulses, followed by measurement of the transverse magnetization. With the pulsed methods, one avoids the problem of the perturbation of the spin system between formation and detection. Furthermore, the sensitivity of the technique can be much higher than that given by TREPR.

The first applications of pulsed EPR in the study of transient free radicals made use of the electron spin–echo (ESE) technique.[4,16,17] With this method, the z magnetization is measured by first rotating it in the xy plane with a $\pi/2$ microwave pulse. This is followed by a delay of a few hundred nanoseconds, after which a π pulse is delivered. The spin–echo signal created by this pulse sequence is a measure of the z magnetization existing at the time the first pulse was delivered. ESE has been applied in two modes. First, the delay τ_d between laser (or radiolysis) pulse and $\pi/2$ pulse can be kept constant and the echo signal measured as function of magnetic field strength. This method gives the spectrum of the radicals present at time τ_d. It should be noted that, as in TREPR, off-resonance signal contributions degrade spectral resolution. Line broadening becomes more pronounced with reduction in microwave pulse width and increase in microwave power (cf. section 2). Second, the echo amplitude can be measured at a fixed field as function of τ_d to determine the time dependence of z magnetization.

Of course, the $\pi/2$ pulse alone generates magnetization in the transverse plane that can serve as a direct measure of z magnetization. In fact, measurement of the free induction decay (FID) of transverse magnetization following a single pulse would be desirable because the ESE signal will not be as strong as the signal given by a $\pi/2$ pulse. Advances in microwave instrumentation during the last decade or so have removed the instrumental limitations that precluded direct measurement of single-pulse-generated FIDs. This led to the application of the FID integration method by Trifunac et al.[18,19] Here the integrated FID serves as a measure of z magnetization present at the time of the microwave pulse. Measurement of this signal as function of magnetic field, at fixed τ_d, gives the EPR spectrum. Measurement at fixed field as function of τ_d gives information on chemical kinetics and spin dynamics. The use of the FID integration method, rather than the equivalent of FT NMR in which Fourier transformation of the FID directly gives the complete spectrum so that a field sweep measurement is superfluous, again was dictated by instrumental constraints.

In recent years a number of research groups have built pulsed-EPR instruments with which it is possible to acquire spectra by measurement of the FID, at fixed field and frequency, followed by Fourier transformation of this time domain signal.[20–23] A commercial pulsed-EPR instrument that can be used for FT EPR measurements also has become available. FT EPR has proven an ideal technique for the study of photochemically generated transient paramagnetic species. The technique offers the ultimate in time and spectral resolution and high sensitivity. Applications have shown that the time evolution of spectra can be monitored over a time regime extending from nanoseconds to milliseconds. Numerical analysis of the spectral data gives (a) the rate constants of formation and decay of free radicals; (b) information on the characteristics of (paramagnetic) reaction precursors that cannot be observed directly; (c) magnitudes of spin polarization generated by CIDEP mechanisms; (d) data on spin relaxation times; and (e) information on molecular motion.

The purpose of this contribution is to review the applications of FT EPR in the study of photochemical reactions. First the instrumental aspects of the method will be summarized. This will be followed by a discussion of the various CIDEP mechanisms that can affect EPR spectra of transient free radicals. Finally, applications of FT EPR in the study of photoinduced electron transfer and hydrogen abstraction reactions will be reviewed. To date measurements have been performed with instruments operating at X-band frequency (~9.5 GHz) only. Recently, Forbes and coworkers[24,25] have reported on TREPR studies performed with a Q-band (~36 GHz) spectrometer. These studies show that measurements employing different microwave frequency bands can be useful in the analysis of CIDEP effects. In considering the potential of Q-band (or even higher frequency) FT EPR, one should keep in mind that the concomitant increase in field strength may give rise to significant line broadening. The field strength effect on T_2 will adversely affect the ability to measure the time domain signal.

2. Instrumental Aspects

A number of FT EPR instruments have been described in the literature.[20–23] It is important to realize that since the technique is the microwave analogue of FT NMR, discussions of the operating principles can be found in texts dealing with pulsed NMR.[26] An excellent discussion of the specific instrumental requirements of FT EPR can be found in the article by Gorcester and Freed.[22] A general discussion of pulsed EPR principles and applications can be found in a recent

article by Schweiger.[27]

As noted in the Introduction, in FT EPR a short microwave pulse rotates the magnetization vector from the external magnetic field (z) axis into the transverse plane. Following the $\pi/2$ pulse, the time evolution of the magnetization in the xy plane (FID) is measured. Fourier transformation of the FID gives the frequency domain EPR spectrum.

Two conditions must be fulfilled for the method to give all frequency components of the spectrum: (1) the inverse of the pulse width (τ_p) must exceed the spectral width; (2) the data sampling rate must be at least twice the frequency of the highest frequency component in the FID.

With a pulse width of τ_p, the microwave field (B_1) required for a $\pi/2$ pulse, assuming that the Larmor frequency of the spin corresponds to the microwave frequency, is given by

$$B_1 = \pi/2\gamma_e\tau_p \quad (1)$$

Here γ_e denotes the gyromagnetic ratio of the electron spin. The B_1 field that can be generated is a function of transmitter power and the power-to-field conversion efficiency of the resonator. The resonators used in instruments described in the literature[20-23] are low-Q cavities with fairly low power conversion efficiency. With 1 kW of transmitter power, a B_1 field of only about 6 G (0.6 mT) may be attained.[22] Then, according to eq 1, a τ_p of at least 14 ns is required for a $\pi/2$ rotation if the spin system is on resonance. For minimal distortion of the spectrum caused by the offset of the resonance frequency ($\omega_{res} = \gamma_e B_0$, where B_0 is denotes the external magnetic field) from the applied microwave frequency (ω_{mw}), the microwave field strength B_1 must meet the requirement

$$|\omega_{res} - \omega_{mw}| \ll \gamma_e B_1 \quad (2)$$

Hence, with B_1 = 6 G, one can expect to measure an undistorted spectrum only if the spectral width does not exceed 12 G (23 MHz). This assumes that ω_{mw} corresponds to the center frequency of the spectrum. On first sight, this appears to severely limit applications of the technique. However, the FID actually carries information covering a considerably broader bandwidth. With B_1 = 6 G, a resonance offset of about 16 G (45 MHz) gives a reduction in signal amplitude of about a factor of 2.[22] One can easily make corrections for the effect the offset has on signal amplitude and phase, so that a broad range of free radicals can in fact be studied.

The frequency range covered by the instrument can be adversely affected by the resonator. To realize the bandwidth coverage given by the microwave field, the resonator bandwidth must be at least as large. This consideration dictates a low resonator Q. A bandwidth coverage of 100 MHz requires that $Q \sim 100$.[22] Since the power-conversion efficiency is reduced by a reduction in Q, the requirement of a large-B_1 field on the one hand, and a wide resonator bandwidth on the other conflict with each other. In instruments that make use of cavities,[20-23] the loss in power conversion efficiency because of deliberate Q spoiling is compensated for by the use of a high-power microwave amplifier (1-kW traveling wave tube amplifier, TWT). With the use of alternative devices, such as the loop-gap[28] and bridged-loop-gap[29,30] resonators, a combination of low Q and high microwave field can be attained at greatly reduced microwave power. Freed and co-workers have used the loop-gap resonator in studies of nitroxides. Their work demonstrates that a spectrum covering a frequency range of 90 MHz or more can be recorded without significant distortion.[31] Generally, the use of standard cavities is preferred because measurements can be made under a broad range of sample conditions. Other resonators may have to be tailor-made to fit the requirements of a given measurement.

The FID is detected by amplification of the microwave signal generated by the sample followed by down conversion of the frequency by mixing with a reference signal from the microwave source. A quadrature IF mixer is used which gives two-channel output. The two signals represent the FID of the magnetization along two orthogonal axes in the xy plane. With this detection scheme ω_{mw} can be set to match the center of the bandwidth one wants to cover because positive frequency deviations can be distinguished from negative deviations. The result is that the bandwidth coverage of the measurement is optimized. A CYCLOPS phase-cycling routine is applied to correct for amplitude and phase errors introduced by the mixer.[26] The signals are sampled with a two-channel data acquisition system. A digital oscilloscope can be used for this purpose.[22,23] The frequency down conversion gives FIDs that can contain frequencies ranging from less than −50 MHz to more than +50 MHz. Hence, the data acquisition device should be capable of two-channel sampling at a rate of at least 100 Ms/s (10 ns/point). The bandwidth of the instrument should be large enough to produce no attenuation of high-frequency signal components. Since a single microwave pulse rarely will produce a signal with sufficient signal-to-noise (S/N), the data acquisition system should be capable of signal averaging.

In FT NMR the spin system generally dictates the repetition rate of the measurement. By contrast, since free radicals in fluid solution relax to thermal equilibrium in microseconds, the pulse repetition rate in an FT EPR measurement is limited by the capabilities of the data acquisition system. With two-channel measurement the upper limit of the repetition rate may be 100 s^{-1}. In photochemical applications, constraints imposed by the sample are likely to set an upper limit on the repetition rate of the measurement.

The FID cannot be measured immediately after the $\pi/2$ pulse because of cavity ring down. For instruments using standard rectangular cavities,[21-23] this deadtime amounts to ~100 ns. The deadtime can be reduced somewhat with the use of a bimodal cavity[20] or loop-gap resonators.[31] If the FID decays fast, the sensitivity of the measurement will be reduced by the deadtime. The rate of exponential damping of the FID (T_2^{-1}) is related to the full width at half-height (ΔW, in hertz of a Lorentzian line by $\Delta W = (\pi T_2)^{-1}$.[26] Thus, the FID of a radical that gives a frequency domain spectrum with peaks with $\Delta W \approx 1$ G will decay to about $1/e$ of its starting amplitude during the spectrometer deadtime. This consideration reveals a serious limitation of the FT EPR technique. Without a significant reduction in deadtime, the technique cannot be used in studies of paramagnetic systems giving resonance peaks with widths much in excess of 1 G.

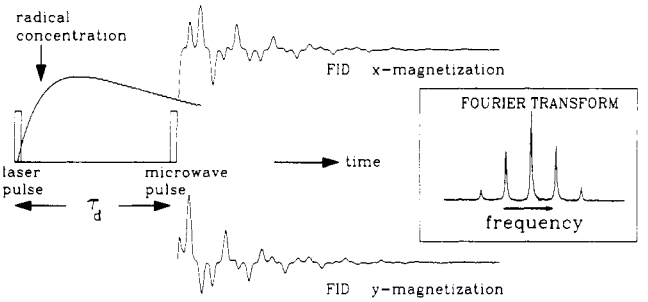

Figure 1. Schematic diagram illustrating the sequence of events in measurements of photogenerated free radicals with FT EPR.

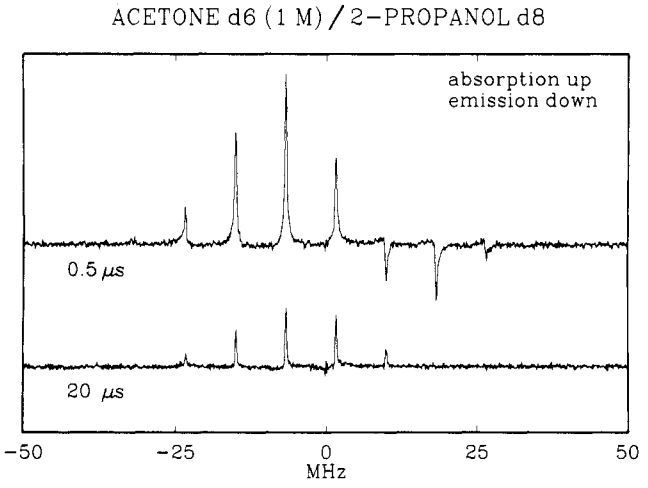

Figure 2. FT EPR spectrum of photogenerated $(CD_3)_2\dot{C}OD$ in acetone-d_6/2-propanol-d_8. Microwave pulse 0.5 and 20 μs after pulsed-laser excitation (308 nm, ~50 mJ/pulse). The total number of laser shots was four (one per phase in the CYCLOPS phase-cycling routine).

The method used in time-resolved studies of photogenerated paramagnetic molecules is presented in Figure 1.[21,32,33] The chemical reaction is initiated by a laser pulse. After a delay τ_d, the $\pi/2$ microwave pulse is delivered and the FID measured. *The FID represents the time-domain spectrum of the paramagnetic species present at the time of the microwave pulse.* Free radicals formed during the time interval the FID is measured—which can cover 10 or more ms—can affect the signal only indirectly through radical–radical interactions. Decay of free radicals during that time is reflected in the form of line broadening in the frequency-domain spectrum.

The high sensitivity and spectral resolution of the measurement is illustrated in Figures 2 and 3. Figure 2 displays the spectrum given by the (perdeuterated) acetone ketyl radical, $(CD_3)_2\dot{C}OD$, formed in the reaction of photoexcited acetone-d_6 with 2-propanol-d_8 for delay times between laser pulse and microwave pulse of 0.5 and 20 μs. Figure 3 shows the central portion of the spectrum from $(CH_3)_2\dot{C}OH$ (~10^{-4} M) generated from nondeuterated compounds. *The spectra were obtained by Fourier transformation of the (average) FID produced by four laser shots. Total acquisition time of a spectrum was 40 μs.* The inset of Figure 3 depicts the multiplet splitting caused by the hydroxyl proton (0.6 G) and second-order effects.

By recording the FIDs for a range of τ_d settings—which can cover 6 orders of magnitude, from nanoseconds to milliseconds—the time evolution of the

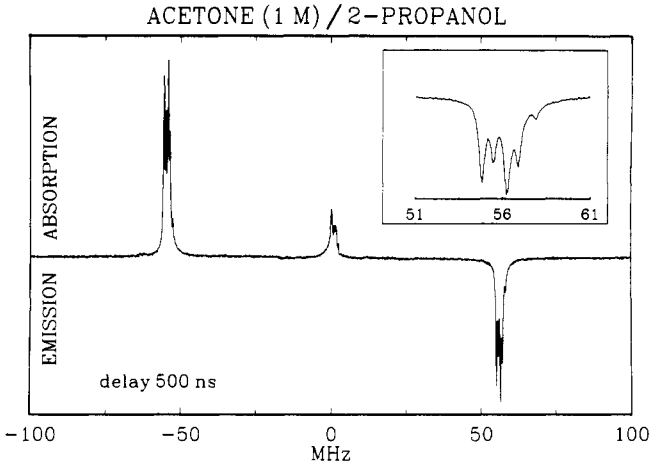

Figure 3. Central portion of the FT EPR spectrum of photogenerated $(CH_3)_2\dot{C}OH$ in acetone/2-propanol. Microwave pulse 0.5 μs after pulsed-laser excitation. The spectra represent an assembly of signals from each one of the three groups of hyperfine lines measured separately by adjusting the field to bring the component of interest on resonance (cf. section 4.1.2). The total number of laser shots used to generate the composite spectrum is 12. The inset illustrates the high resolution of the measurement.

spectra from photogenerated free radicals can be monitored. Of interest in these studies is the time dependence of all spectral parameters: frequencies, amplitudes, line widths, and phases of all peaks in the spectrum. The information can be derived from the frequency-domain spectra obtained by Fourier transformation of the FIDs. However, since it is contained as well in the original time-domain signal, the Fourier transformation step is superfluous. Instead, spectral data can be extracted directly from the FIDs with a linear prediction-singular value decomposition (LP-SVD) analysis routine.[34,35] The procedure is based on the assumption that, to a good approximation, the FID can be represented by the sum of a number of exponentially damped sinusoids:

$$S_n = \sum_{k=1}^{l} c_k \exp[-\alpha_k + (i2\pi\nu_k)n\Delta t + \phi_k] \qquad (3)$$

Here, l is the number of sinusoids, and c_k, α_k, ν_k, and ϕ_k stand for the amplitude, damping, frequency, and phase of the kth sinusoid, respectively. The sampling interval is Δt and the nth data point is measured at time $n\Delta t$. LP-SVD directly gives numerical data for the spectral parameters for each τ_d setting so that a computer analysis of the time dependence of each one of the parameters is facilitated. If the data analysis method involves Fourier transformation of the FID as the initial step, the data points missed because of the instrument deadtime can cause artifacts in the frequency-domain spectrum which can make it difficult to extract reliable data.[26] Because LP-SVD can be applied on any set of data points in the FID, the deadtime problem can be avoided. The analysis of the time-domain signal can also be performed with a nonlinear least-squares routine that uses the variable projection (VARPRO) method. The VARPRO analysis can be applied not only on exponentially damped sinusoids but also on any function that describes the decay of the time-domain signal.[35]

3. CIDEP Mechanisms

The spin system of photochemically generated radicals generally will not be at thermal equilibrium at the time of formation. For instance, if a pair of doublet-spin free radicals is formed by bond scission, one could (naively) assume that each radical initially will have equal α and β spin-state populations. In that case, if the EPR spectrum is recorded before complete relaxation of the system, the signal amplitude will be less than that obtained for the same number of radicals at Boltzmann equilibrium. The time evolution of the spectrum will reflect chemical kinetics as well as spin-lattice relaxation. Since spin–lattice relaxation times (T_1^R) of free radicals in solution typically are of the order of microseconds, spectra from species formed a few microseconds prior to the measurement will show deviations from thermal equilibrium. Chemical decay of free radicals also can give rise to deviations from thermal equilibrium. EPR spectra can be affected by this effect for an extended time period.

The fact that signal amplitude is determined both by chemical processes and spin dynamics vastly complicates the analysis of time-resolved spectra. However, the effort spent provides a great deal of information on the mechanisms of reactions. To a large extent, this information is not accessible to other spectroscopic techniques. Hence, detailed time-resolved EPR studies can give unique insights.

The processes that create non-Boltzmann electron spin polarization in paramagnetic molecules are collectively known as chemically induced dynamic electron polarization (CIDEP) mechanisms. A number of reviews concerned with CIDEP effects have been published in recent years.[3-6] In the following, an overview of the various CIDEP mechanisms and their effects on EPR spectra will be given.

3.1. Triplet Mechanism

Triplet mechanism (TM) spin polarization in doublet radicals can be generated if their formation involves a precursor in a photoexcited triplet state:[36,37]

$$^1M \xrightarrow{h\nu} {}^1M^* \xrightarrow{isc} {}^3M^*$$

$$^3M^* + Q \rightarrow {}^2R_1 + {}^2R_2$$

Photoexcited triplets are formed by intersystem crossing (isc) from an excited singlet state. The isc process is spin selective and creates spin polarization in the triplet-state molecules.[38,39] If the chemical reaction is fast enough to compete with triplet spin–lattice relaxation, the triplet spin polarization will be carried over to the doublet radicals.

The isc process is governed by selection rules imposed by the symmetry characteristics of the singlet and triplet excited states involved.[38,39] Experimentally, the spin polarization created by isc can be determined with magnetic resonance measurements.[38,39] Of interest here is that precursor triplets may have populations in the T_{+1} and T_{-1} spin states that deviate from Boltzmann equilibrium at the time of the reaction. If spin conservation rules apply, T_{+1} triplets will give α spin-state doublet radicals and T_{-1} triplets β spin radicals. Then, an excess population in the T_{+1} level will give excess population in the α level producing a stimulated-emission EPR signal. If the reverse is true, an enhanced absorption signal is observed. Since the mechanism is independent of nuclear spin state, relative intensities of peaks, given by hyperfine interactions between electron spin and nuclear spins, remain unaffected by this CIDEP mechanism.

With a triplet spin–lattice relaxation time of T_1^T and a pseudo-first-order radical formation rate constant k_f, the time development of the TM CIDEP signal contribution is given by

$$S_{TM} = \frac{k_f P_T}{k_f + T_1^{T-1}}\left[1 - \exp\left\{-\left(k_f + \frac{1}{T_1^T}\right)t\right\}\right] \quad (4)$$

where P_T represents the initial difference in population of the T_{-1} and T_{+1} triplet states. The expression shows that transfer of triplet spin polarization requires that $k_f \geq 1/T_1^T$. T_1^T of triplet state molecules in fluid solution is determined by modulation of the dipole–dipole interaction between the unpaired electrons due to molecular motion. Values are expected to be in the nanosecond range.[40,41] Hence, reaction rates of the order of 10^8–10^9 s^{-1} are required for creation of TM CIDEP. This is a stringent requirement that may not be always fulfilled.[42]

The identification of a TM spin-polarization contribution in the EPR of photochemically produced free radicals establishes the involvement of a precursor triplet molecule in the reaction. A complete analysis of the TM signal contribution will yield the value of the triplet spin–lattice relaxation time and the magnitude of the spin polarization in the triplets. This information is difficult to extract from spectra obtained with TREPR because data for the early time domain, where the generation of TM CIDEP can be monitored directly, are hard to obtain and, if obtained, difficult to interpret for reasons pointed out in the Introduction. The fact that TREPR does not provide direct, unequivocal, evidence of TM CIDEP has made the question of whether or not the mechanism can be observed in certain systems a matter of dispute.[6,42] To quote from the section dealing with TM CIDEP (ref 6, section 4.1.1, p 315) of a recent review of TREPR applications by McLauchlan, "There is little doubt that the triplet mechanism is the source of single-phase hyperfine-independent polarization in many cases, but it is not obvious that this is always so, although to date all spectra have been interpreted on this basis."

With FT EPR, the time evolution of spectra during the first few hundred nanoseconds following a laser pulse can be monitored readily.[32,33,43,44] They provide unambiguous evidence of TM contributions and have been used to determine T_1^T. That it proved feasible to measure the spin–lattice relaxation time and spin polarization in precursor triplets, which are EPR silent under the conditions of the measurements, is of considerable interest since these parameters reflect the molecular tumbling of the triplets. Hence, they provide information on medium effects on molecular motion. This can, for instance, be useful in studies of photochemical reactions in microheterogeneous environments.[45]

It should be noted that reactions involving triplet precursors may give rise to hyperfine-independent, non-

Boltzmann, spin polarization in doublet radical products for other reasons as well. First, the population difference, at thermal equilibrium, between T_{-1} and T_{+1} spin states is approximately twice as large as that between the β and α spin states in the doublet radical. Hence, a reaction involving triplets at thermal equilibrium will produce free radicals that initially should give enhanced-absorption EPR signals. Second, spin polarization can be produced by a triplet-sublevel-dependent reaction rate.[46] In either case, the polarization can be distinguished from that produced by spin-selective isc on the basis of the difference in kinetics. TM CIDEP develops with a rate determined by chemical kinetics and T_1^T. Contributions from the other two mechanisms reflect chemical kinetics only.

3.2. Radical Pair Mechanism

The formation of free radicals in a photochemical reaction involves a transient radical pair. For instance, in an excited-state electron-transfer reaction

$$D^* + A \rightarrow {}^{1,3}[D^+\cdots A^-] \rightarrow D^+ + A^-$$

The initial spin state of the radical pair, $[D^+\cdots A^-]$, can be singlet or triplet depending on the spin state of the excited-state precursor D*. The radical pair spin state evolves in time because of the difference in precession frequencies of the two unpaired electrons.[47] The spin-state evolution gives rise to what is known as radical pair mechanism (RPM) CIDEP. The difference in precession frequencies can be caused by a difference in g value and/or the effect of hyperfine interactions. Since the mixing terms are small compared to the Zeeman interaction, appreciable singlet–triplet mixing during the time the two radicals stay correlated, generally, can occur only between the singlet (S) and triplet T_0 states of the pair. Even for the S–T_0 states, spin-state evolution during the time the radicals are in close contact is expected to be too small to give rise to CIDEP in most cases. Normally, the mixing terms are small compared with the S–T_0 splitting caused by the exchange interaction J between the unpaired electrons. Instead, the generation of RPM spin polarization in low-viscosity solvents can be accounted for with a three-step process.[48,49] In the first step, the reaction produces a contact radical pair. In the second, the radicals diffuse apart so that $J \sim 0$ and ST_0 mixing is effective. In the third, the radicals reencounter, and the effect of the mixing is expressed in the form of excess α spin character for one radical and a concomitant excess in β spin character for the other. The one-step—encounter followed by cage escape—mechanism of ST_0 CIDEP[47] can play a role in systems where radical pair lifetime is long, for instance, in high-viscosity solvents.[6]

The theoretical expression for ST_0 RPM spin polarization in radical 1 in nuclear spin state a because of interaction with radical 2 in nuclear spin state b is given by[49]

$$P_1^{ab} = C[Q_{ab}{}^{1/2} - \gamma Q_{ab}] \quad (5)$$

Here Q_{ab} represents half the difference in resonance frequencies of radicals 1 and 2 and is given by

$$Q_{ab} = {}^1/_2\{\mu_B B\Delta g + \sum_m a_{1m} m_{1m}^a - \sum_n a_{2n} m_{2n}^b\} \quad (6)$$

The g value difference is given by Δg, hyperfine interactions in radicals 1 and 2 by a_{1m} and a_{2n}, respectively. The spin quantum number of the mth (nth) nucleus of radical 1 (2) in overall nuclear spin state a (b) is given by m_{1m}^a (m_{2n}^b). In a calculation of the RPM CIDEP spectrum of radical 1, one sums over contributions from all possible nuclear spin states of radical 2 taking nuclear spin-state degeneracy (d_b) into account:

$$P_1^a = \sum_b d_b P_1^{ab}$$

The first term in eq 5 represents the contribution from the reencounter process, the second the encounter–dissociation sequence. Under most conditions $\gamma \sim 0$. The value of the proportionality constant C is a function of the mean time between relative diffusive displacements of the radicals. The sign of C depends on the sign of J and the spin state of the excited-state precursor molecule. Generally, $J < 0$ then, for triplet-state precursors, low-field hyperfine peaks will be in emission and high-field peaks in absorption. For reactions involving singlet excited-state precursors, the pattern is reversed.

Overall, the ST_0 RPM does not create net spin polarization. Under special conditions, ST_{-1} mixing can make a contribution and in that case RPM CIDEP will have a net polarization component. As pointed out earlier, this will generally not play a role because the energy gap between S and T_{-1} states, induced by the external magnetic field, is large compared to the mixing terms. However, if hyperfine coupling is strong or the radical pair is captured in a suitable configuration, so that there is near degeneracy of the S and T_{-1} states, ST_{-1} CIDEP contributions can be observed.[50-52] Theory predicts that this mechanism gives an emission spectrum if the excited-state precursor is a triplet, and an absorption spectrum is given by a singlet excited-state precursor.[4-6] The method of calculating the polarization given by this mechanism is described in the review of TREPR by McLauchlan.[6]

Since the perturbation terms producing singlet–triplet mixing depend on the nuclear spin state, relative intensities of hyperfine components differ from those given by nuclear spin state degeneracy. In this respect, RPM CIDEP differs from TM CIDEP. Given sufficient time resolution, TM CIDEP also can be distinguished from RPM CIDEP on the basis of the time evolution of the two contributions. According to eq 4, the development of the TM signal component depends, in part, on the value of T_1^T. RPM spin polarization will be generated during the entire course of the free-radical formation step. It is of interest that normally the dominant component of RPM CIDEP depends on a separation–reencounter mechanism. Hence, it must have a characteristic rise time that, in principle, should be observable at early times ($\tau_d < 20$ ns) in time-resolved EPR spectra.

So far the focus has been on spin polarization produced in the free-radical formation step, it involves geminate radical pairs. Chemical decay caused by random encounters of free radicals also generates RPM spin polarization.[4-6] Encounters giving singlet-state pairs are reactive leaving triplet radical pairs which are subject to the same spin-state evolution processes as geminate pairs. It follows that random encounters give

rise to the same spin polarization as triplet geminate pairs and that its magnitude can be evaluated with eqs 5 and 6. The contribution to RPM CIDEP produced by random encounters of radicals is labeled F-pair spin polarization.

From the foregoing, it is clear that RPM CIDEP can be a source of information on the mechanism of radical formation. It can be used to determine the spin state of precursor molecules and the characteristics of radical pairs.

3.3. Spin-Correlated Radical Pairs

The preceding discussion has been concerned with the effects of spin dynamics in paramagnetic precursors on the spectrum of free radicals. In special cases radical pairs can live long enough so that they can be observed directly with time-resolved EPR,[45,53-57] TREPR,[53-55] and FT EPR[45,57] spectra of these spin-correlated radical pairs (SCRP) are characterized by a derivative-like line shape. This unusual spectral feature is accounted for as follows.[53,54] It is assumed that the radicals in the pair are weakly coupled so that the exchange interaction between the unpaired electrons is small compared to the difference in resonance frequency ($\Delta\omega = \omega_1 - \omega_2$) of the two radicals. In that case the spectrum of the pair—ignoring hyperfine splittings for the moment—will consist of two pairs of lines centered at ω_1 and ω_2 with a doublet splitting of $2J$. In a first-order approximation, the spin functions of the pair are given by

$$\chi_1 = \alpha_1\alpha_2, \quad \chi_2 = \alpha_1\beta_2 + \lambda\beta_1\alpha_2$$

$$\chi_3 = \beta_1\alpha_2 - \lambda\alpha_1\beta_2, \quad \chi_4 = \beta_1\beta_2$$

The mixing parameter λ is small because of the condition $\Delta\omega \gg J$. To first order, a pair of lines can be associated with transitions in one of the two radicals. For instance, $\chi_3 \rightarrow \chi_1$ and $\chi_4 \rightarrow \chi_2$ give the doublet spectrum due to radical 1. If the observed pair is formed non-adiabatically from a strongly coupled pair with singlet spin state, then only χ_2 and χ_3 will be populated. As illustrated in Figure 4, for $J < 0$ the low-field line of each doublet will be in absorption whereas the other will be in emission. If the pair is created initially in the triplet state, χ_1 and χ_2 each carry one-third of the spin population, whereas the middle two levels share the remaining one-third. Now χ_2 and χ_3 are less populated than the other two states so that the doublets will display an emission/absorption pattern (cf. Figure 4). With the value of J of the order of the line width—and also taking into account that there may be a distribution of J values[54]—the doublet splitting will not be resolved. Instead, the partial merging of absorption and emission peaks will produce a derivative-like signal for each of the hyperfine components in the spectrum.

A special case arises in pulsed-EPR measurements if SCRPs dissociate into free radicals in the interval between delivery of the microwave pulse and recording of the ensuing signal.[23,58-60] Figure 5 illustrates the time development of the magnetization for one of the two radicals in the pair. In a FT EPR measurement, the microwave pulse rotates the magnetization vectors of the two distinct spin states, created by the interaction with the second electron spin, in the plane perpendicular

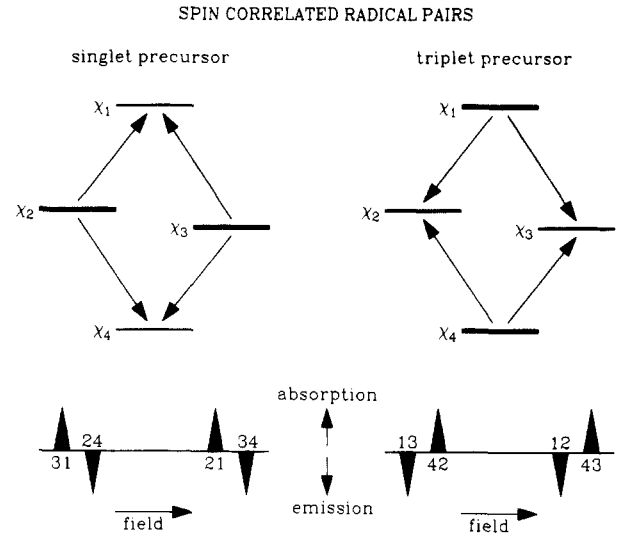

Figure 4. Schematic energy level diagram of a radical pair. The relative populations of the spin states given by singlet and triplet precursors, respectively, are indicated by the thickness of the lines marking the four spin states. The radical-pair EPR spectra for the case that $|J| \ll \Delta\omega$ are sketched below the energy level diagram. See text (section 3.3) for further details.

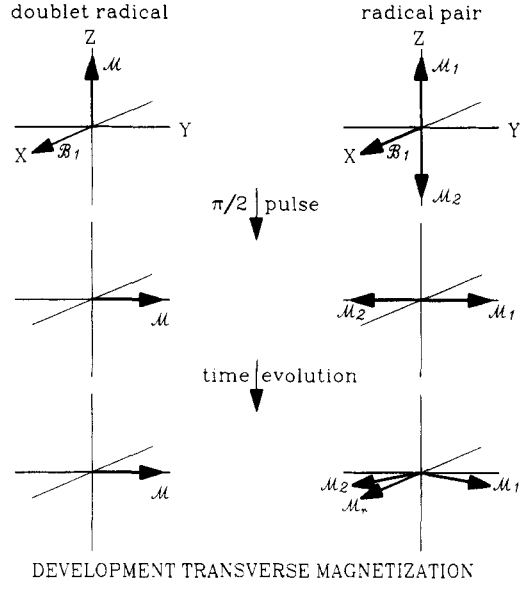

Figure 5. Comparison of the time development of the magnetization given by a doublet radical and by the same radical experiencing weak exchange coupling with a second radical. The magnetization is presented in a coordinate system that rotates with a frequency corresponding to the resonance frequency of the unperturbed radical. The microwave field B_1 used for $\pi/2$ rotation of magnetization is directed along the x axis. See text (section 3.3) for further details.

to the static magnetic field. The vectors are of equal magnitude, but point in opposite directions. Hence, contrary to the result obtained for a spin $^1/_2$ system, the $\pi/2$ pulse does not produce net magnetization in the xy plane. Following the pulse, the two vectors precess around the z axis. Because the precession frequency is determined in part by the spin state of the second radical, transverse magnetization—along an axis perpendicular to that characterizing normal absorption or emission signals (cf. Figure 5)—is produced. This out-of-phase or dispersion signature is carried along by the

radicals upon dissociation of the pair. Hence, even though the lifetime of SCRPs may be too short for them to contribute directly to the FID, the growth, and decay of these species can be determined with a measurement of the time dependence of the amplitude of the dispersion signal.[23,59,60]

Superficially, the derivative-like signals produced by direct observation of SCRPs and the dispersion component carried over to the signals from free radicals are similar in appearance. In principle, the two can be distinguished on the basis of line widths since peaks in spectra from SCRPs contain the unresolved exchange interaction splitting. With TREPR only direct observation of SCRPs is possible, so a comparison of results obtained with cw and pulsed-EPR techniques can be useful for interpretation of derivative-like signal contributions. It must be stressed that both kinds of radical pair signals actually can be observed with pulsed-EPR only if the turning angle of the magnetization vector is $<\pi/2$.[57]

3.4. Polarization from Doublet–Quartet Mixing

Recent studies[61-65] show that the interaction between excited-state molecules and stable free radicals—such as nitroxide spin labels—can produce spin polarization. The first reports concerned with the effect of photoexcited triplets on the EPR spectrum of doublet radicals.[61,63,64] The interaction between triplet- and doublet-state molecules in fluid solution was found to give emission spectra. In principle, the spin polarization can arise from simple spin polarization transfer from triplets.[61] However, this mechanism is not expected to be very effective because it must compete with fast spin–lattice relaxation of the triplets. In fact, FT EPR measurements carried out in this laboratory[66] demonstrate that the polarization builds up with a rate matching the rate of diffusion-controlled encounters between triplet and doublet radicals. This result is in accord with the proposal by Blättler et al.[63] that polarization is produced in a doublet–quartet spin-state mixing process similar to the process that gives rise to RPM CIDEP. In this case, however, the dominant mixing term is the dipole–dipole (zero-field-splitting, zfs) interaction between the unpaired electrons in the triplet. As predicted by theory,[63,64] the magnitude of the polarization increases with increasing zfs terms. Encounters between excited-singlet molecules and free radicals can give rise to enhanced-absorption signals[65] as a result of doublet–quartet mixing. TREPR spectra showing this effect have been reported.[65] Since the relative magnitudes of the effects depends critically on the singlet excited-state lifetime, both effects can be observed in the TREPR spectra of suitably chosen systems. Enhanced absorption is found shortly after laser excitation because of the interaction of the radicals with singlet excited-state molecules. Emission signals are observed for longer delays, at which time the contribution from the longer-lived triplets is at a maximum.[65]

While this mechanism of spin polarization creation does not involve a chemical reaction—and therefore cannot be classified as a CIDEP mechanism—it is clear that it can play a role in studies of photochemistry with time-resolved EPR. Efforts to enhance the signal from photogenerated free radicals (high solute concentration, high laser power) may inadvertently lead to conditions where the mechanism gives a significant signal contribution.

4. Applications

4.1. Photoinduced Electron Transfer

The majority of FT-EPR studies of photochemical reactions have dealt with excited-state electron transfer. Investigations have focused primarily on the reversible photoreduction of quinones by porphyrins. Electron transfer from porphyrins to quinones has been studied in homogeneous solution at various temperatures[32,33,43,44,59,60,67,68] and as function of solvent composition.[69] Measurements have been performed as well on porphyrin/quinone in micellar solutions[45,70] and adsorbed in the pores of silica gel.[71] An FT EPR and TREPR study has been made of a covalently linked carotenoid–porphyrin–diquinone tetrad.[57] A recent publication is concerned with the study of electron transfer from zinc and free-base octaethylporphycenes to quinones.[72] A few studies deal with electron transfer from amines to quinones.[21,73] Finally, a paper by Levanon and co-workers discusses a FT-EPR investigation of photoinduced electron transfer from the pyrene dianion to alkali metal cations.[74]

In the following discussion the utility of the FT EPR technique in this field of research will be illustrated with examples drawn primarily from investigations of porphyrin/quinone systems.

4.1.1. FT EPR Studies of Porphyrin/Quinone in Homogeneous Solution

ZnTPP/Duroquinone in Ethanol. A number of studies have been concerned with the reversible photoinduced electron transfer from zinc tetraphenylporphyrin (ZnTPP) to duroquinone (DQ)[32,33,43,44,67] in ethanol. Figure 6 gives a series of spectra obtained in a study of ZnTPP (5×10^{-4} M)/DQ (5×10^{-3} M) in ethanol at −28 °C. The delay time between laser excitation (600 nm, 2 mJ/pulse) and $\pi/2$ microwave pulse ranges from 10 ns to 80 μs. The spectrum observed is that of the duroquinone anion radical (DQ^-). The cation radical cannot be observed because of the fact that unresolved hyperfine structure gives broad lines so that the FID decays within the deadtime of the spectrometer. Under steady-state conditions, the EPR spectrum of DQ^- consists of 13 lines with binomial intensity distribution because of hyperfine coupling with 12 equivalent protons (1.9 G[75]). Figure 6 shows that there is a strong delay-time dependence of both the overall signal amplitude and the relative amplitudes of hyperfine components. For τ_d up to about 1 μs there is rapid overall signal growth. In this time period, the spectrum, which initially is in absorption, gradually turns into a spectrum in which the high-frequency (low-field) peaks are in emission. With τ_d increasing from 1 to 80 μs the signal intensity diminishes and emission peaks turn back into absorption, eventually giving the normal binomial intensity distribution.

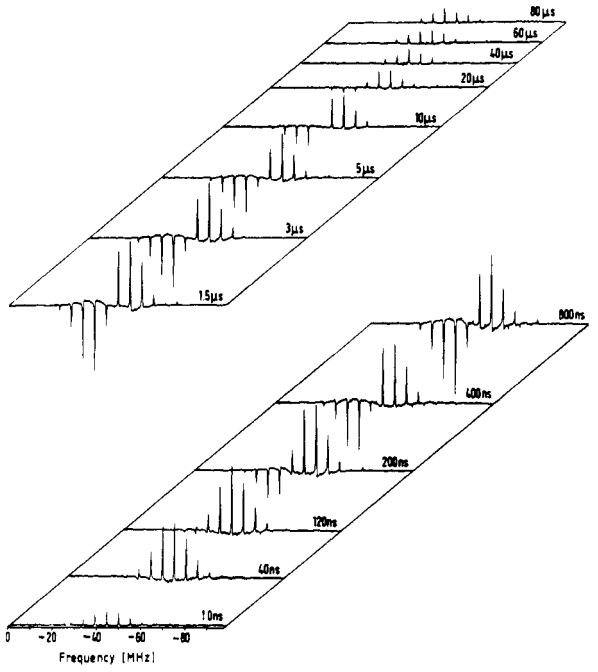

Figure 6. FT EPR spectrum of DQ^- produced by photoinduced electron transfer from ZnTPP to DQ in ethanol at −28 °C. Delay time between laser pulse and microwave pulse ranges from 10 ns to 80 μs. Reprinted from 30; copyright 1988, American Chemical Society.

The results can be accounted for within the framework of the following reaction mechanism:

$$ZnTPP \xrightarrow{h\nu} {}^1ZnTPP^* \xrightarrow{isc} {}^3ZnTPP^* \quad (7)$$

$$^3ZnTPP^* + DQ \xrightarrow{k_{et}} [ZnTPP^+\cdots DQ^-] \xrightarrow{k_{ce}} ZnTPP^+ + DQ^- \quad (8)$$

$$ZnTPP^+ + DQ^- \xrightarrow{k_d} ZnTPP + DQ \quad (9)$$

The signal growth reflects the kinetics of electron transfer from $^3ZnTPP^*$ to DQ. The ZnTPP triplets are formed in a spin-selective isc process that produces excess population in the T_{-1} spin state.[76] Hence, DQ^- formed before the triplet spin system is at thermal equilibrium will show an enhanced-absorption (TM) component. Electron transfer involving the T_0 triplet state will generate ST_0 RPM polarization which is associated with a low-field/high-field E/A pattern. From the data presented in Figure 6 it is deduced that TM CIDEP dominates at early times ($\tau_d < 200$ ns). As the triplet spin system relaxes, the RPM signal contribution gains in relative importance. Consequently, low-field hyperfine lines which are initially in absorption turn into emission. The conclusion that the TM gives a significant contribution is illustrated convincingly by the finding that the polarization pattern changes when the donor molecule is MgTPP[43] or free-base TPP.[66] In these porphyrins the isc process gives a triplet system with excess population in the T_{+1} level so that the TM gives rise to an emission signal.

TM spin polarization gives equal contributions to pairs of hyperfine lines with overall nuclear spin states M and $-M$. Therefore, the time evolution of the RPM signal contribution is given by the difference in signal amplitudes (ΔS_M) of M and $-M$ hyperfine lines. In the time regime from 0 to 0.5 μs the RPM signal, to a good approximation, reflects the formation of DQ^- so that the signal growth can be used to determine the rate of free-radical formation. This method of analysis gave pseudo first-order rate constants of 7.7×10^6, 1.5×10^7, and 2.2×10^7 s^{-1} at −23, 0, and 27 °C, respectively.[67] Within experimental error the rate is proportional to temperature/viscosity (T/η). From this it was concluded that the reaction rate is diffusion controlled.

The decay of the ΔS_M signals reflects spin–lattice relaxation and back-electron transfer. Under the experimental conditions, the first process is expected to be the dominant decay channel for $\tau_d < 20$ μs. From the signal decay it was determined that the spin–lattice relaxation time (T_1^R) of DQ^- ranged from 4.5 μs at 27 °C to 10.4 μs at −23 °C.[67]

Finally, the value of the spin-lattice relaxation time T_1^T of the triplet and the magnitude of the TM polarization were determined from the time dependence of the $M = 1$ hyperfine peak for $\tau_d < 150$ ns. It can be shown that the RPM gives a small contribution to this peak so that signal growth, to a good approximation, is represented by eq 4 (section 3.1). A least-squares fit of the experimental data to eq 4 gave 50, 40, and 20 ns for T_1^T at −23, 0, and 27 °C, respectively. The theoretical expression for TM polarization relative to the Boltzmann value, P_{eq}, is[37]

$$\frac{P_T}{P_{eq}} = \frac{4kT\omega_{zfs}}{30\, g\beta B\omega_{mw}} \frac{T_1^T}{(T_1^T + k_{et}^{-1})}[2P_z - P_x - P_y] \quad (10)$$

In this equation B denotes the field strength, ω_{mw} and ω_{zfs} the microwave frequency (9.5 GHz) and zero-field-splitting (1 GHz), respectively. P_x, P_y, and P_z give the relative rates of population of the zero-field triplet spin states. For ZnTPP isc almost exclusively populates the $|z\rangle$ level so that $P_z \approx 1$.[39,77] From eq 10 one derives $P_T/P_{eq} = 5$. This agrees quite well with the value of 6 derived from the experimental data. Under conditions that the polarization is not attenuated by relaxation, i.e., $T_1^T \gg k_{et}^{-1}$, TM spin polarization would amount to $22P_{eq}$.

An FT-EPR study of ZnTPP/DQ in ethanol by Bowman et al.[43,44] employed a more comprehensive method of data analysis in that the time dependence of individual hyperfine components was analyzed. The data given by these authors for the most part are in agreement with those from the Dortmund group[32,33,67] except for the value of 460 ns given for T_1^T.[43] A detailed study of ZnTPP/BQ ethanol solutions with four different BQ concentrations, in which the time evolution of the amplitudes of three hyperfine lines in the BQ^- spectrum were used to determine rate constants, gave $T_1^T = 28 \pm 10$ ns at room temperature[68,69] in agreement with the result reported by Plüschau et al.[67]

Spin-Correlated Radical Pairs. The LP-SVD analysis (cf. section 2) of the FIDs given by ZnTPP/DQ in ethanol shows that there is a pronounced out-of-phase signal component for $\tau_d < 300$ ns.[59,60] The effect is attributed to the presence of spin-correlated radical pairs at the time the microwave pulse is delivered. Under the conditions of the measurement, SCRPs have vanished for the most part by the time the FID is collected. However, as pointed out in section 3.3, the

exchange interaction between the unpaired electrons of the pair in the interval between microwave pulse and signal detection generates a characteristic phase shift in the FID of the free radicals.[58-60] Kroll et al. studied the time evolution of the out-of-phase signal intensity at temperatures ranging from −48 to 25 °C.[60] It was found that the data could be described with a model in which the formation and decay of the pairs follows first-order kinetics. The rate of radical-pair generation was found to match the rate of free-radical formation. The rate of dissociation k_{ce} ranged from 3.2×10^6 s^{-1} at −48 °C to 1.0×10^7 s^{-1} at 25 °C. In a low-viscosity solvent such as ethanol, free translational diffusion of the redox ions would give a much shorter SCRP lifetime (4–40 ns) than measured experimentally. The long lifetime has been interpreted in terms of a model that assumes that an attractive potential of the order of a few kT restricts relative motion of the radicals.[60,78] In [ZnTPP$^+$···DQ$^-$], the electrostatic interaction between the redox ions obviously can account for restricted diffusive separation. The interpretation of the experimental data in terms of Shushin's model[78] yields a dielectrically-screened binding potential of ~2.6 eV.[60]

The information on SCRPs derived from FT-EPR data gives a direct insight into the role played by solvent molecules in the outcome of the excited-state electron transfer process. An increase in solvent dielectric constant will reduce the depth of the potential well that traps the radical pairs and thereby increases the probability of cage escape of redox products.

A more pronounced solvent effect on SCRP characteristics was reported recently in a paper on a FT-EPR study of the anthraquinone/triethylamine photoredox system.[73] In this study the kinetics of photoinduced electron transfer was monitored via the spectrum of the antraquinone anion radical (AQ^-). An order of magnitude reduction in the rate constant of AQ^- formation was found upon going from methanol to 2-propanol as solvent. The reduction cannot be accounted for solely by the change in solvent viscosity. Instead it is proposed that the rate-limiting step in free-radical formation is cage escape. Considering the high donor concentration used in the study (5×10^{-2} M), this assumption seems well justified. The spectra do not show an out-of-phase signal from SCRPs, and it is assumed that this is due to strong exchange interaction between unpaired electrons in the pair. The strong solvent dependence is attributed to the modulation of radical pair lifetime by binding potential changes induced by changes in solvent dielectric constant.

It is noteworthy that the AQ^- spectra initially are in emission and do not show RPM CIDEP. The emission signal is attributed to TM spin polarization. This implies that at least some of the polarization carried over from triplet precursors remains preserved in the radical pairs even though they have relatively long lifetimes (for example, in propanol a radical pair lifetime of 563 ns is found).

ZnTPP/BQ in Ethanol. In a study of ZnTPP/BQ in ethanol[68,69] the effect of acceptor concentration on electron-transfer kinetics and spin dynamics was investigated. As in the study by Plüschau et al.,[67] values for the electron-transfer and BQ^- spin–lattice relaxation rates were derived from the time dependence of the

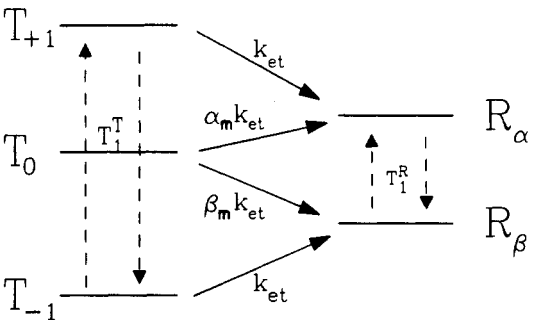

Figure 7. Schematic diagram illustrating the processes that control the time evolution of spin state populations in anion radicals formed by photo-induced electron transfer from a triplet precursor. See text (section 4.2.1) for details. Reprinted from ref 65; copyright 1992, American Chemical Society.

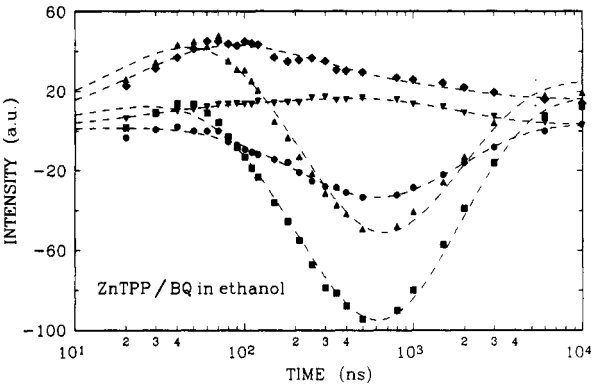

Figure 8. Time evolution of the intensities of the hyperfine components (▼ +2, ◆ +1, ▲ 0, ■ −1, ● −2) in the BQ^- spectrum. The dashed lines represent the results of least-squares fits of the data using equations describing spin dynamics based on the model given in Figure 7. Reprinted from 65; copyright 1992, American Chemical Society.

difference in signal intensities of $M = 1$ and -1 ($M = 2$ and -2) peaks. With the values of these two parameters known, values for spin polarization parameters and T_1^T were derived with a least-squares analysis of the time dependence of individual hyperfine components over the time regime from 20 ns to 10 μs. The model used in the analysis is presented in Figure 7. It takes into account (1) spin polarization in precursor triplets, (2) T_1^T, (3) spin conservation in BQ^- formation from T_{-1} and T_{+1} triplet states, (4) RPM CIDEP in the form of an electron- and nuclear-spin-dependent electron-transfer rate constant from the triplet T_0 state, and (5) T_1^R. Note that the numerical analysis gives the rate of formation of BQ^- (in nuclear spin state M) with β ($\beta_M k_{et}$) and α spin ($\alpha_M k_{et}$), where $\beta_M + \alpha_M = 1$ (cf. Figure 7). The value of $(\beta_M - \alpha_M)$ represents ST_0 spin polarization. The analysis does not take back electron transfer into account, since it is assumed to make a minor contribution in the time interval that is considered. A representative result of this method of data analysis is given in Figure 8. It displays a plot of the amplitudes of the five hyperfine lines in the spectrum of BQ^- for a range of τ_d values and the result of a least-squares fit based on the kinetic model sketched in Figure 7.

The study showed that the electron-transfer rate is a function of BQ concentration. An upper limit for the pseudo-first-order rate constant is attained with [BQ] ≥ 3.0×10^{-3} M. Apparently, the condition is reached

where the rate of formation of free BQ^- is determined by the rate of dissociation (k_{ce} in eq 8) of radical pairs rather than the rate of encounter of donor and acceptor molecules. With [BQ] = 3.0×10^{-3} M, the reaction rate is 1.2×10^7 s^{-1}. If it assumed that this rate represents k_{ce}, one finds a radical pair lifetime of 83 ns. The value is in close agreement with the result of the more direct measurement[60] of radical pair formation and decay discussed earlier.

Radical pair characteristics, evidently, play an important role in determining the outcome of donor–acceptor encounters. The fact that radical pair lifetime can be measured with EPR, therefore, is of considerable interest. Since radical pairs, generally, cannot be distinguished from separated radicals with UV–vis spectroscopy, optical measurements do not provide this information.

For [BQ] < 3×10^{-3} M, division of the measured pseudo-first-order rate of formation of BQ^- by [BQ] also does not yield an invariant second-order electron-transfer rate constant. The rate constant shows an increase from 3.6×10^9 to 5.5×10^9 M^{-1} s^{-1} as the acceptor concentration increases from 0.6 to 2.0 mM. A similar concentration effect was found in studies of fluorescence quenching reactions which proceed with rates that are close to diffusion controlled.[79-82] The effect has been attributed to the fact that the concentration gradient driving the reactions extends to a distance from the excited state molecule which is a function of quencher concentration.[81,82] Stevens proposes that the concentration gradient extends only to a distance corresponding to the initial most probable nearest-neighbor separation r_{nm} between quencher and excited-state molecules. Introduction of this boundary condition in the solution of the flux equation gives the following expression for the quenching rate constant:[81]

$$k_q = \frac{4\pi NDR}{1 - R/r_{nn}} \qquad (11)$$

N is Avogadro's number, D is the relative diffusion coefficient, R is the quenching radius, and $r_{nn} = [2\pi Nc]^{-1/3}$, where c is the quencher concentration. The equation reverts to the Smoluchowski equation[83] for $r_{nn} \gg R$ ($c \rightarrow 0$).

It was found that the expression accounts satisfactorily for the concentration dependence of the second-order rate constant of BQ^- formation for 0.6 mM ≤ [BQ] ≤ 2.0 mM. The analysis gives $(2.00 \pm 0.05) \times 10^9$ M^{-1} s^{-1} for the rate constant of electron transfer under the condition that $R \ll r_{nn}$, i.e., for [BQ] → 0. This result agrees with data from optical studies of ZnTPP/BQ.[84,85] A value of 30 Å is found for the reaction radius R. The parameter defines the maximum center-to-center distance between ^{3}ZnTPP* and BQ at which quenching will occur. A detailed paper on a TREPR study of ZnTPP/BQ in ethanol[86] gives a rate constant of 1.25×10^9 M^{-1} s^{-1} at −43 °C. It is noteworthy that this study does not find an acceptor concentration dependence of the rate constant.

The study also revealed an *apparent* acceptor concentration dependence of T_1^R. The decay rate of the ΔS_M signals increases from 4.4×10^5 to 8.0×10^5 s^{-1} upon going from [BQ] = 0.6 to 3.0 mM. The result demonstrates that the decay of the ΔS_M signals cannot be attributed solely to spin–lattice relaxation. A concentration dependent process that contributes to the decay is the homogeneous electron-transfer reaction:[87]

$$BQ^- + BQ \xrightarrow{k_{het}} BQ + BQ^- \qquad (12)$$

Homogeneous electron transfer provides, what is in essence, a nuclear spin relaxation path that redistributes the overall electron spin polarization. It drives the relative intensities of the hyperfine components to the 1:4:6:4:1 pattern. Taking this process into account, the rate of decay of ΔS_M signals is given by

$$k_\Delta = k_{T_1^R} + k_{het}[BQ] \qquad (13)$$

Analysis of the concentration dependence of ΔS_M signals with the aid of eq 13 (taking nuclear spin state degeneracy into account) gives $k_{het} = 1.65 \times 10^8$ M^{-1} s^{-1} and $T_1^R = 2.3$ μs. The interpretation of the concentration dependence of signal decay is supported by the finding that the line widths of the hyperfine components in the spectrum of the anion radical increase with increasing [BQ]. Homogeneous electron transfer gives rise to a lifetime-broadening contribution to the line width (at half-height expressed in hertz) of $\Delta W_{het} = k_{het}[BQ]/\pi$.[88] The concentration dependence of the line width gives $k_{het} = (3.2 \pm 1.2) \times 10^8$ M^{-1} s^{-1}, the linewidth for [BQ] = 0 is 0.26 ± 0.05 MHz (0.09 G).

An alternative method that can be used in the measurement of homogeneous electron transfer has been reported by Angerhofer et al.[89] These authors measured the rate constant of electron transfer between photogenerated duroquinone anion radicals DQ^- and DQ in methanol with a two-dimensional FT EPR method. The rate constant for this system (1.5×10^8 M^{-1} s^{-1}) is very similar to that found for the BQ^-/BQ couple in ethanol.

An analysis of the time dependence of the intensities of three hyperfine peaks in spectra given by ZnTPP/BQ samples with four different BQ concentrations (ranging from 0.6 to 1.6 mM) gave $T_1^T = 28 \pm 10$ ns. The initial spin polarization of the ^{3}ZnTPP* triplets relative to thermal equilibrium was found to be 22 ± 2. The result is in excellent agreement with the value predicted by theory and the result derived from the study of ZnTPP/DQ.[67] The relative amplitudes of hyperfine components due to RPM CIDEP derived from the spectra are −2.1:−6.9:−6.0:−0.88:+0.39 (the results are given in order of increasing field, negative values denote emission signals). Relative intensities given by ST_0 spin polarization can be calculated with eqs 5 and 6 (section 3.2). For $\gamma = 0$, the calculated values are −1.8:−5.9:−6.0:−1.1:+0.5.[87] The systematic deviation between experimental and theoretical values suggests that the second term in eq 5 cannot be neglected. This conclusion is supported by the finding that a reduction in temperature enhances the deviations. The TREPR study of ZnTPP/BQ in ethanol by Schlüpmann et al. also finds evidence of a ST_{-1} signal contribution.[86] The values of the RPM spin polarization relative to Boltzmann polarization are −42, −35, −20, −4.1, and +8.1.

ZnTPPS/BQ in Water/Ethanol. Measurements were performed as well on ZnTPPS/BQ in H_2O/ethanol solvent mixtures.[69] ZnTPPS refers to zinc tetraphenylporphyrin with SO_3^- substituents in the para position of the phenyl rings. The objective of the investigation

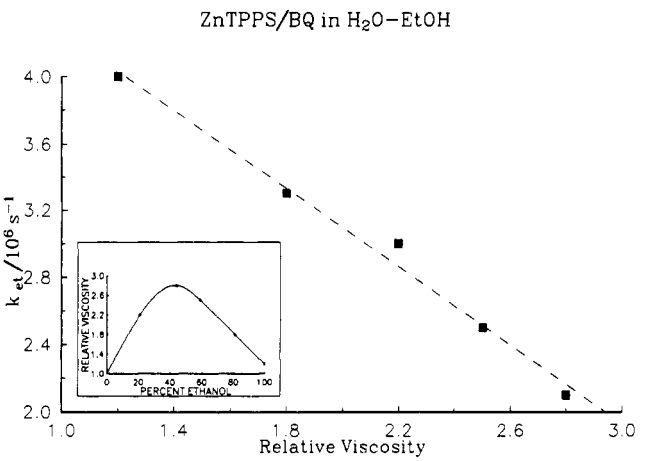

Figure 9. Pseudo-first-order rate of formation of BQ^- by photoinduced electron transfer from ZnTPPS (2×10^{-4} M) to BQ (10^{-3} M) in H_2O/ethanol mixtures plotted versus solvent viscosity (relative to the viscosity of H_2O). The first data point (relative viscosity ≈1.2) gives k_{et} obtained for ZnTPP/BQ in ethanol. The inset displays the relation between relative viscosity and solvent composition percent ethanol by weight). From ref 66.

was to get information on the effect of solvent changes on chemical kinetics and spin dynamics. In addition, the measurements were used to probe the effect of modification of Coulomb interaction between redox ions.

Measurements on ZnTPPS (2×10^{-4} M) with BQ (10^{-3} M) in H_2O/ethanol showed that the chemical decay of BQ^- is slower than that found for ZnTPP/BQ in ethanol. Also, little or no evidence was found for a radical pair signal contribution. These results reflect the fact that electrostatic repulsion between the anionic redox products tends to keep them apart. As Figure 9 shows, with the solvent composition changing from 20% to 80% ethanol, the pseudo-first-order rate of electron transfer closely follows changes in solvent viscosity. As depicted in the inset in Figure 9, viscosity changes are not linearly related to changes in solvent composition. The result demonstrates that, at the acceptor concentration used, the reaction rate is proportional to the rate of encounter of donor and acceptor molecules. The changes in solvent polarity accompanying changes in solvent composition apparently have little effect on the rate of BQ^- formation. Another noteworthy finding is that the value for k_{et} found for ZnTPP/BQ in ethanol also fits the straight-line dependence of rate on viscosity displayed in Figure 9. Thus, the introduction of the sulfonate groups on the periphery of the porphyrin molecule has no significant effect on the reaction rate. This supports the conclusion that the rate of encounter is the determining step in the BQ^- formation.

4.1.2. FT EPR Study of Porphyrin/Quinone in Heterogeneous Media

A study has been made of ZnTPP/BQ in a micellar solution of cetyl trimethyl ammonium chloride (CTAC)[70] and of ZnTPPS/DQ in micellar solutions made up of anionic, cationic, or neutral surfactant molecules.[45] The interest in these systems stems in part from the potential relevance to applications in conversion and storage of solar energy.[90,91] Also, studies of these systems can contribute to the understanding of the factors that play

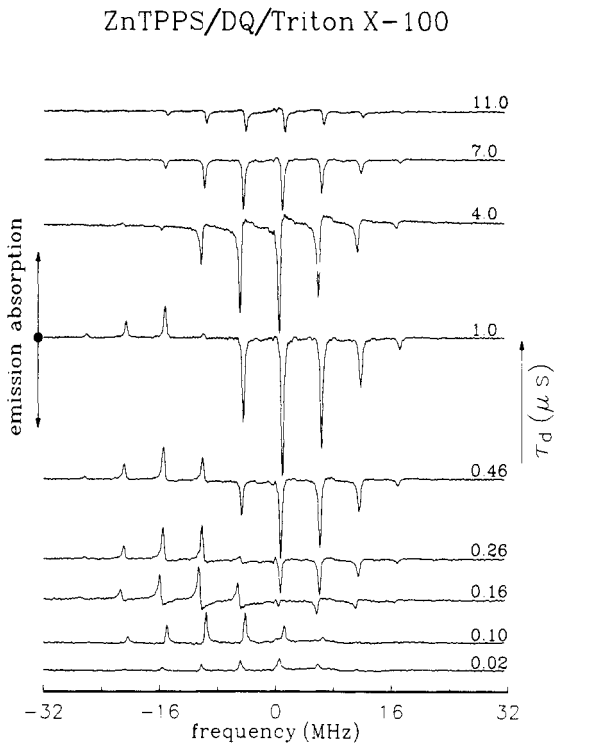

Figure 10. FT EPR spectra of photogenerated DQ^- in TX100 solution for delay times between laser excitation of ZnTPPS and microwave pulse ranging from 20 ns to 11 μs. The central hyperfine line ($M = 0$) is at ≈−4.5 MHz. Reprinted from ref 43, copyright 1988, Weizman Science Press.

a role in electron transfer across boundaries between hydrophobic and hydrophilic domains. The key point of these FT EPR studies is that they exploit the fact that CIDEP contributions, line shapes, line widths, and relaxation times are sensitive to the spatial distribution of reactants and products, and motional correlation times. Hence, FT EPR measurements can give a unique insight into structure and dynamics.

ZnTPPS/DQ in Micellar Solutions. The study of ZnTPP/BQ in CTAC showed that electron transfer mainly occurred from ZnTPP solubilized in the micelles to BQ in the aqueous phase.[70] In the case of ZnTPPS/DQ, acceptor molecules are captured in the micelles while the location of the anionic porphyrin depends on the charge of the polar headgroup of the surfactant molecules. For this system, changes in surfactant molecules are found to have a profound effect on the FT EPR spectra.[45]

Figure 10 depicts the time evolution of the FT EPR spectrum of DQ^-, in a Triton X-100 (TX100) solution, generated by photoinduced electron transfer from ZnTPPS. The spectra are qualitatively similar to those found for ZnTPP/DQ in ethanol.[67] At early times (τ_d < 100 ns) a TM CIDEP contribution dominates which establishes that the reaction involves ZnTPPS triplets. For τ_d > 100 ns RPM CIDEP dominates; here the low-frequency absorption/high-frequency emission pattern also is consistent with triplet excited-state electron transfer.

Contrary to what was found in homogeneous solution, the growth of the RPM signal—a measure of free-radical formation—cannot be represented by a single exponential. Instead, it appears to involve two consecutive steps with first-order rate constants of 1.7×10^7 and 1.4×10^6 s^{-1}. This suggests that the kinetics of DQ^-

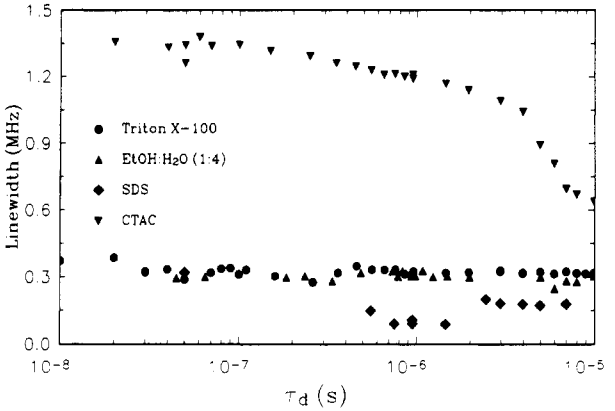

Figure 11. Time evolution of the linewidth ($\Delta\nu = 1/\pi T_2$) of the central line in the spectra from DQ^- in TX100 (●), CTAC (▼), and SDS (◆). The line width of the $M = 0$ line in the spectrum from BQ^- in H_2O/ethanol (4:1) (▲) is given for comparison. Reprinted from ref 43, copyright 1988, Weizman Science Press.

formation reflects the radical pair formation step as well as the cage-escape step. Even the fastest of the two steps has a rate constant smaller than the value of $2.2 \times 10^7\ s^{-1}$ found for ZnTPP/DQ ([DQ] = 5×10^{-3} M) in ethanol. The result is surprising because acceptor as well as donor molecules are associated with the micelles.[92] It is estimated that the average distance between reactants is less than 20 Å compared to ~38 Å for the ZnTPP/DQ in ethanol system. With such a short distance between reactants, one would expect fast electron transfer, with a significant singlet excited-state contribution. Instead, the spectral data show a relatively slow reaction with no evidence of DQ^- formation via the singlet excited state. However, the fluorescence of ZnTPPS in TX100 is quenched appreciably by the addition of DQ. It is concluded, therefore, that electron-transfer singlet quenching does occur but does not yield free DQ^- because of fast back electron transfer. Singlet-state quenching must involve closely spaced reaction partners so that the average spacing between ^{3}ZnTPPS* and DQ can be substantially larger than 20 Å. This can account for the relatively slow rate of triplet excited-state electron transfer.

An analysis of the time evolution of the TM CIDEP contribution shows that T_1^T is 100–150 ns, a factor of 4 longer than in homogeneous solution. The T_1^T value is consistent with the conclusion that ZnTPPS is associated with the micelles. Molecular motion in the micelles will be inhibited which is expected to increase the spin–lattice relaxation time. On the other hand, T_1^R of DQ^- is similar to the value found in ethanol. In addition, the line widths of the hyperfine lines match those found in homogeneous solution (cf. Figure 11). Restricted molecular motion inside the micelle and interaction with the porphyrin radical would cause severe line broadening. Hence, the findings indicate that the anion radicals move into the aqueous phase. A slight reduction in line width with increase in delay between laser pulse and microwave pulse, apparent for $\tau_d < 100$ ns may reflect the movement of DQ^- across the micelle/water interface.

The spectrum from ZnTPPS/DQ in sodium dodecyl sulfate (SDS) micellar solution displayed in Figure 12 is very similar to that found for ZnTPPS/DQ in homogeneous solution as well. The main differences

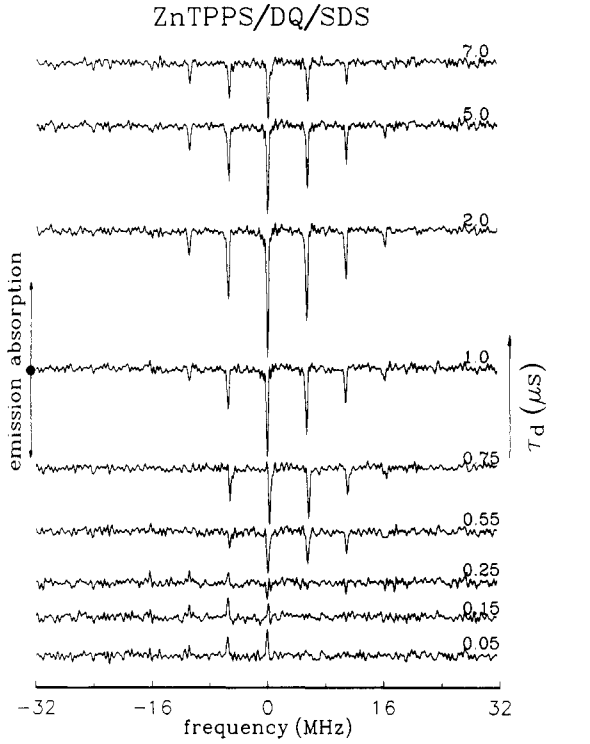

Figure 12. FT EPR spectra of photogenerated DQ^- in SDS solution for delay times between laser excitation of ZnTPPS and microwave pulse ranging from 50 ns to 7 μs. The central hyperfine line ($M = 0$) is at ≈0 MHz. Reprinted from ref 43, copyright 1988, Weizman Science Press.

with the results obtained with ZnTPPS/DQ in TX100, for the same concentrations of donor and acceptor, are (1) a significant reduction in signal and (2) a reduced rate of DQ^- formation. The differences can be accounted for by the difference in reactant distribution in the heterogeneous solutions. In SDS the ZnTPPS molecules are found in the aqueous phase rather than inside the micelles.[92] Hence, electron transfer must involve encounters of ^{3}ZnTPPS* molecules with the few DQ molecules that are in the aqueous phase as well. The compartmentalization of reactants leads to a reduction in the pseudo-first-order reaction rate.

Fluorescence measurements show that, in SDS solution, ^{1}ZnTPPS* quenching by DQ is significant. Optical absorption spectra indicate that this is due to ground-state complexation. Apparently, singlet excited state quenching does not generate free DQ^- and, by diminishing the ^{3}ZnTPPS* concentration, reduces the EPR signal intensity.

Data obtained from ZnTPPS/DQ in CTAC solution are given in Figure 13. It is evident that the DQ^- spectrum for $\tau_d < 5$ μs differs substantially from that found with the other micelles. All hyperfine lines exhibit a derivative-like line shape in this time regime. The lineshape bears a striking resemblance to that found in the FT EPR spectrum from the photoreduced quinone moiety in a covalently-linked donor–acceptor tetrad.[57] A similar line shape has been found in TREPR spectra of photogenerated radicals in viscous and micellar solutions.[53,54] The unique line shape is a manifestation of the presence of SCRPs [$ZnTPPS^{3-}$···DQ^-]. In this case the radical pairs are observed directly, i.e., they are present at the time the FID is recorded. As explained in section 3.3, a weak exchange interaction—in this case of the order of 1

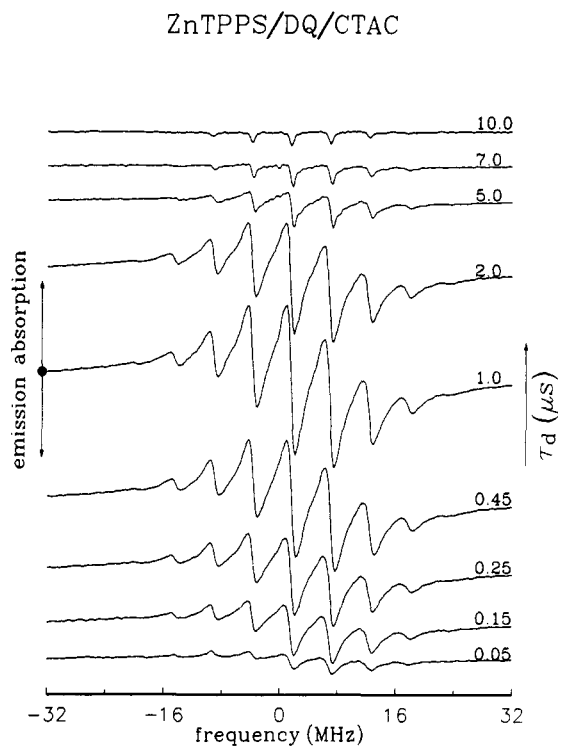

Figure 13. FT EPR spectra of photogenerated DQ^- in CTAC solution for delay times between laser excitation of ZnTPPS and microwave pulse ranging from 50 ns to 10 μs. The central hyperfine line ($M = 0$) is at ≈7 MHz. Reprinted from ref 43; copyright 1988, Weizman Science Press.

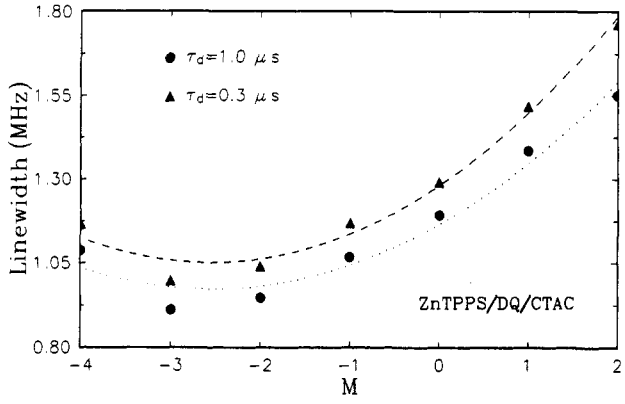

Figure 14. Dependence of the line width ($\Delta\nu_M = 1/\pi T_2(M)$) on the total nuclear spin quantum number for DQ^- in the ZnTPPS/DQ/CTAC system for τ_d settings of 0.3 μs (▲) and 1.0 μs (●). The dashed and dotted lines represent the least-squares fittings of the data points to eq 14. The coefficients (in megahertz) derived from the fits are a = 1.28 (1.16), b = −0.18 (−0.15), and c = 0.035 (0.03) for τ_d = 0.3 (1.0) μs. Reprinted from ref 43; copyright 1988, Weizman Science Press.

MHz or less—between the unpaired electrons splits every hyperfine line into an unresolved doublet. The doublets exhibit a low-frequency absorption/high-frequency emission pattern, consistent with formation via a triplet-state precursor (cf. Figure 4). By contrast, in the covalently linked donor–acceptor system electron transfer involves the singlet excited state and the radical pair spectrum displays an emission/absorption pattern.[57] The formation and decay of the radical pair spectrum can be described reasonably well with single exponentials ($k_1 = 3.6 \times 10^6$ s^{-1}, $k_2 = 5.0 \times 10^5$ s^{-1}). In CTAC, as in TX100, electron transfer is between reactants associated with the micelles.[92] The long lifetime of SCRPs—the maximum signal amplitude is given for $\tau_d \approx 0.8$ μs—is attributed to interaction between the anionic reaction products and the positive electrostatic field generated by the cationic headgroups of surfactant molecules. The interaction inhibits relative translational diffusion of the redox products.

The spectrum of free DQ^- is observed when $\tau_d > 5$ μs. At that time the spectrum still reflects spin polarization (most hyperfine components are in emission, cf. Figure 13). From the decay of the polarization it is deduced that T_1^R of DQ^- in CTAC is ~8 μs as compared to 4.5 μs in TX100 solution. Figure 11 shows that the linewidth in the spectrum of "free" DQ^- in CTAC solution also is significantly larger than in TX100 and SDS. These results indicate that the anion radicals remain trapped in the cationic micelles.

Figure 14 shows that the linewidths in the spectrum of the SCRP is a function of nuclear spin state (M) of DQ^-. The M dependence can be described by the polynomial

$$\Delta\nu_M = a + bM + cM^2 \qquad (14)$$

Values of the coefficients a, b, and c derived from a least-squares analysis of the line width data are given in the caption of Figure 14. The M dependence is attributed to incomplete averaging of g and hyperfine anisotropies by rotational motion.[93,94] The rotational correlation time τ_R can be derived from the coefficients with the aid of the theoretical expressions given in the paper by Suga et al.[94] The τ_R value derived from b and c are 10.5 and 3.3 ns, respectively. The paper by Leniart et al. gives the experimentally determined values of b and c as function of τ_R for DQ^- in ethanol.[93] With an extrapolation of their results, values of 24 and 10 ns are derived from the two coefficients. It is concluded that the line-width data point to strongly inhibited rotational motion of the radicals. For comparison, τ_R = 2.3 ns for DQ^- in ethanol at −70 °C.[93] The systematic deviation between the rotational correlation times derived from the two coefficients can be due to nonrandom rotational motion of DQ^- as a result of the interaction with the electrostatic field inside the micelles.

ZnTPP/BQ Adsorbed on Silica Gel. There is considerable current interest in photochemistry involving reactants adsorbed on solid supports such as silicagels and zeolites.[95] This is because it is known that the unique spatial organization and motion of reactants, imposed by the solid support, will be reflected in reaction kinetics and mechanisms. It can be exploited to enhance the yield of desired products and to attenuate processes that adversely affect photochemistry.

Time-resolved EPR is an ideal spectroscopic technique for this field of research for all the reasons that have been delineated in the foregoing. Of particular interest is, of course, the possibility to probe molecular motion of transient paramagnetic species and the characteristics of radical pairs. Two recent publications by Forbes et al.[24,25] demonstrate the value of TREPR studies of photochemistry at the solid/liquid interface of SiO_2 surfaces.

Research in this laboratory has been concerned with photoinduced electron transfer from ZnTPP to BQ adsorbed in the pores of silica gel (Davisil 634, 60-Å pore). Because the electron-transfer process is reversible, this is a convenient system to investigate with FT

EPR as it does not require sample flow through the cavity. Here some preliminary results will be reviewed.[96]

Sample preparation followed the procedure given by Johnston et al.[97] Typically, a solution of ZnTPP and BQ in hexane/dichloromethane (3:1) was mixed with silica gel and stirred for 1 h. The adsorption of donor and acceptor was monitored with UV–vis absorption spectroscopy. After filtration and washing of the filtrate with hexane, the solid was dried in an argon atmosphere. Subsequently, solvent was introduced by exposing the solid to a flow of solvent-saturated argon. Solvent uptake was monitored by weighing. If it is assumed that all the donor and acceptor molecules end up in the solvent captured in the silica gel pores, their concentrations are estimated to be 6 and 60 mM, respectively. Sample tubes were stoppered by septum caps to prevent sample exposure to oxygen.

In the presence of oxygen, fluorescence of ZnTPP adsorbed on silica gel is strongly quenched. Also, only a weak spectrum of ^{3}ZnTPP* can be obtained with TREPR and this required cooling of the sample to −100 °C or lower. Purging of ZnTPP/silica samples with argon restored ZnTPP fluorescence. Furthermore, with these purged samples, TREPR spectra of triplet-state ZnTPP could be observed even at room temperature. Observation of EPR spectra of triplets signifies that rotational motion of the porphyrin is essentially stopped. TREPR measurements of ZnTPP/silica samples purged with solvent-saturated argon reveal a triplet EPR spectrum only at reduced temperature. Apparently, adsorption of solvent molecules restores the motion of the porphyrin. This finding is of importance, since it implies that at room temperature donor and acceptor molecules have some motional freedom in silica gel pores as long as solvent molecules are present.

"Dry" ZnTPP/BQ/silica samples and ZnTPP/BQ/silica samples saturated with hexane did not give photoinduced FT EPR spectra. If excited-state electron transfer does occur, the back reaction must be so fast that redox ion products cannot be detected. By contrast, samples exposed to methanol or ethanol gave well-resolved FT EPR spectra from photogenerated BQ^-.

Figure 15 depicts the spectrum from BQ^- obtained from a ZnTPP/BQ/silica sample saturated with methanol. The time dependence of peak intensities is displayed in Figure 16. The time evolution has the following characteristics: (1) the rise time of the signal is close to instrument limited (50 ns), (2) the spectrum at early times is in enhanced absorption, (3) signals persist into the millisecond time domain, and (4) for τ_d values up to tens of microseconds, the FIDs display unusual phase effects and deviations from the binomial intensity pattern are observed even in the millisecond time domain (cf. insets of Figures 15 and 16).

From the fact that the signal initially is in enhanced absorption it is deduced that separated free radicals are formed by triplet excited-state electron transfer. The rise time of the TM signal component (~50 ns) shows that the spin–lattice relaxation time of ^{3}ZnTPP* is similar to that found in homogeneous solution,[67,68] which is indicative of free rotational motion of the donor. The relatively small RPM contribution grows in with

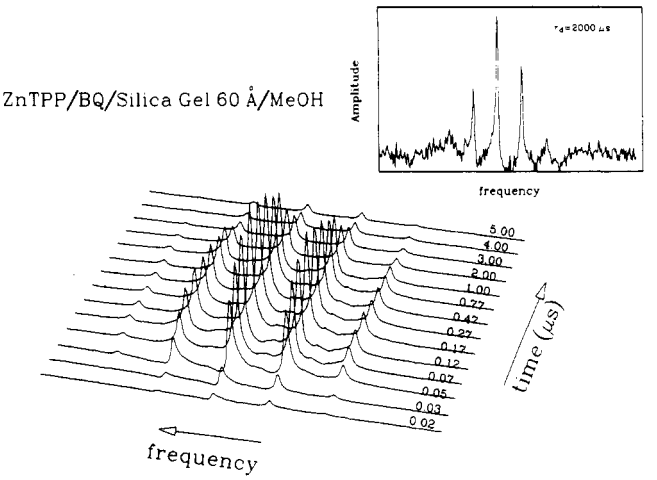

Figure 15. FT EPR spectra from BQ^- formed by electron transfer from ZnTPP to BQ adsorbed in silica gel (pore size 60 Å, pores filled with methanol). The inset depicts the spectrum obtained with τ_d = 2 ms. From ref 68.

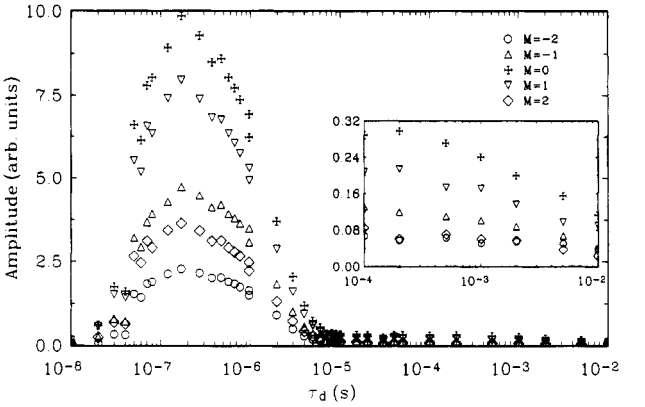

Figure 16. Time dependence of the intensities of the five hyperfine components in the spectra from BQ^- given in Figure 15. The inset highlights the dependence for long delay times. From ref 68.

a rate of about 1.5×10^7 s^{-1} when the solvent is methanol and 0.8×10^7 s^{-1} with ethanol as solvent. These values are approximate because the time evolution of the signals is not purely exponential. The unusually fast signal rise time shows that BQ^- formation must involve reaction partners that are closely spaced at the time of laser excitation of ZnTPP. The change in solvent also is accompanied by a substantial increase in linewidth (from ~1 to 3 MHz). For comparison, the linewidth found for ZnTPP/BQ in ethanol is 0.26 MHz.[68] The large line width in the silica/alcohol environment can be due to a number of factors: there can be a line-width contribution from spin–spin interaction between redox partners, incomplete averaging of hyperfine and g value anisotropies may play a role, and homogeneous electron transfer is expected to affect the line width.

A striking result is that the signal from BQ^- is generated with a time constant which is appreciably smaller than that found for ZnTPP/BQ in ethanol[68] On the other hand, a fraction of the free radicals formed persists for a very long time. These, apparently contradictary, results can be explained by considering sample constitution. First, the acceptor concentration is high so that homogeneous electron transfer (eq 12) can play an important role. Electrostatic interaction between redox partners and restrictions imposed by the heterogeneous medium are expected to inhibit

charge separation, but these effects may be overcome by the homogeneous electron transfer process. Second, only ZnTPP molecules near the surface of the silica gel particles are accessible to the laser light. As a consequence, electron transfer must occur near the surface. Following electron transfer, translational diffusion and homogeneous electron transfer can move a fraction of the anion radicals over macroscopic distances to the interior of the silica gel particles. Back electron transfer involving these anions is expected to be a slow process.

Signal decay in the time interval from 200 ns to 10 μs is reasonably well described by a single exponential with a time constant of $\approx$1 μs. The decay is attributed to establishment of thermal equilibrium by spin–lattice relaxation. The fact that T_1^R is more than a factor of two shorter than that found in homogeneous solution[68] probably is due to spin–spin interaction with the cation radical.

It must be stressed that in the application of FT EPR in the study of photochemistry in heterogeneous media the standard methods of analysis of FIDs may not reveal all the information contained in the time-domain signal. For instance, in the recording of the FID from DQ^- generated by electron transfer from ZnTPPS to DQ in micellar solution (or in the pores of silica gel), radical pairs may dissociate into free radicals or DQ^- may move from hydrophobic to aqueous phase. Evidently, the FIDs contain a complete record of these changes in characteristics of the paramagnetic species. The extraction of the information from the time-domain signal will require development of appropriate methods of data analysis.

4.2. Acetone Ketyl Radical

The formation of the acetone ketyl radical, $(CH_3)_2\dot{C}OH$ by photoinduced hydrogen abstraction from 2-propanol proved to be an ideal subject for FT EPR study for two reasons. First, numerous earlier EPR studies[12,42,53,55,98-108] provide information on kinetics of formation and decay, as well as on CIDEP mechanisms under a variety of conditions. Therefore, there is a base of information that can be used to gauge data derived from FT EPR spectra. Second, acetone ketyl radical formation continues to be a topic of ongoing investigations because of some unresolved questions concerning CIDEP signal contributions.[6,107,108] The high time resolution and sensitivity of FT EPR makes it possible to contribute to the resolution of these questions.[23,109] In the following, results from previous work will be reviewed briefly. This will be followed by a discussion of data from FT EPR investigations.

4.2.1. Background

$(CH_3)_2\dot{C}OH$ can be formed in the reaction between photo-excited acetone and 2-propanol (2Pr). From the rate of formation of $(CH_3)_2\dot{C}OH$ it can be concluded that the singlet-excited state of acetone cannot play a significant role in the reaction.[110] The H-abstraction reaction, therefore, involves the following steps:

$$(CH_3)_2CO \xrightarrow{h\nu} {}^1(CH_3)_2CO^* \xrightarrow{isc} {}^3(CH_3)_2CO^*$$

$$^3(CH_3)_2CO^* + (CH_3)_2CHOH \rightarrow [(CH_3)_2\dot{C}OH\cdots(CH_3)_2\dot{C}OH] \rightarrow 2(CH_3)_2\dot{C}OH \quad (15)$$

Chemical decay of $(CH_3)_2\dot{C}OH$ can occur via pinacol formation:

$$2(CH_3)_2\dot{C}OH \rightarrow HO(CH_3)_2CC(CH_3)_2OH \quad (16)$$

and disproportionations:

$$2(CH_3)_2\dot{C}OH \rightarrow (CH_3)_2CHOH + CH_2{=}C(CH_3)OH \quad (17)$$

$$2(CH_3)_2\dot{C}OH \rightarrow (CH_3)_2CHOH + (CH_3)_2C{=}O \quad (18)$$

At room temperature pinacol formation accounts for about 25% of the decay.[111]

In EPR studies, a solution of acetone in 2Pr, purged with nitrogen or argon, is pumped through a flow-EPR cell. The radicals are formed in situ by irradiation with UV light. With steady-state irradiation the spectrum observed is that of a spin system at thermal equilibrium. It consists of seven peaks with binomial intensity distribution arising from hyperfine interaction with the six equivalent methyl protons (a_H = 19.7 G). High-resolution spectra reveal further splittings due to the hydroxyl proton (0.7 G) and second-order effects.[98]

Time-resolved EPR spectra, in principle, can show CIDEP from the TM and RPM. As discussed in section 3.1, TM spin polarization will give a single-phase (absorption or emission) signal contribution in which the relative intensities of hyperfine components are identical to those found at thermal equilibrium. If radical formation involves photoexcited triplets, ST_0 RPM CIDEP will give a spectrum with inversion symmetry with the three low-field peaks (nuclear spin projections M = 3, 2, 1) in emission, the high-field lines (M = −3, −2, −1) in absorption, and the center line with zero intensity.

Paul[12] studied the kinetics of the reaction and the spin polarization created by radical formation and decay with cw EPR. The study used modulation of the intensity of a light source in conjunction with phase-sensitive detection of the EPR signal. Data on chemical and spin dynamics is derived from the light modulation frequency dependence of the amplitude and phase of the signals. Paul finds no evidence for TM CIDEP and gives values of $\approx$20 and $\approx$60 for the geminate- and F-pair spin polarization of the M = 1 hyperfine peak. The RPM CIDEP values have been questioned[4,19] because they are based on a value for the spin–lattice relaxation time of $(CH_3)_2\dot{C}OH$ (T_1^R = 0.94 μs) which is about a factor 3 lower than the value obtained in TREPR[106] and pulsed-EPR studies.[4,19]

TREPR measurements show that the spectrum of $(CH_3)_2\dot{C}OH$ contains a single-phase absorptive signal contribution, in addition to the E/A contribution from ST_0 CIDEP, even for τ_d < 1 μs.[42,100,102] The origin of the single-phase contribution has become a point of dispute. Paul's study[12] indicates that this signal component arises because spin polarization from thermalized acetone triplets is transferred to the doublet radical. Transfer of Boltzmann polarization from a triplet spin system will give doublet radical polarization that is $^4/_3$ times the thermal equilibrium value P_{eq}. On the other hand, a detailed study of the system by Yamauchi et al.[102] concludes that the absorptive contribution stems from TM CIDEP. In a later study,[104]

these authors give a value of $8P_{eq}$ for the polarization that gives rise to the enhanced-absorption signal.

The conclusion that TM CIDEP gives a noticeable signal contribution has been questioned for the following two reasons. First, the acetone triplet spin–lattice relaxation rate—estimated to be $\sim 2.5 \times 10^8$ s^{-1} [102]—exceeds the pseudo-first-order rate constant of H abstraction ($\sim 10^7$ s^{-1} [106]) by about a factor of 25. As a consequence, according to eq 4, TM polarization will be $^1/_{40}$ times the initial triplet polarization P_T. Second, the EPR spectrum from acetone triplets[112] indicates that TM CIDEP should give rise to an emissive signal.

On the basis of TREPR studies, McLauchlan and co-workers[6,42,107] also conclude that there must be an enhanced-absorption signal contribution with a non-equilibrium spin polarization of $\sim 7P_{eq}$. However, the Oxford group provides evidence that the signal cannot be due to TM CIDEP. For instance, an enhanced-absorption signal of similar magnitude is found when the ketyl radical is formed in a reaction of 2Pr with *tert*-butoxy radicals given by photocleavage of *tert*-butyl peroxide:[107]

$$(CH_3)_3COOC(CH_3)_3 \xrightarrow{h\nu} 2(CH_3)_3C\dot{O}$$

$$(CH_3)_3\dot{C}O + (CH_3)_2CHOH \rightarrow (CH_3)_2\dot{C}OH + (CH_3)_3COH \quad (19)$$

Since radical formation in this case does not involve a triplet excited-state precursor, it is evident that TM CIDEP cannot play a role. To account for their observations, McLauchlan and co-workers propose that an, as yet unidentified, mechanism is responsible for the polarization.[107]

Studies also have been concerned with the radical pair $[(CH_3)_2\dot{C}OH\cdots(CH_3)_2\dot{C}OH]$[55,104,106] TREPR spectra from acetone ketyl radicals in 2Pr show derivative-like signal contributions at low temperature (<–40 °C). These have been attributed to the presence of SCRPs in solution at the time of signal detection.[55,104,106] The origin of the unusual lineshape has been discussed in section 3.3. The spectroscopic data show that the radical pairs have a longer lifetime than that predicted by a model of free diffusional motion given the bulk viscosity of the solvent. To account for the long lifetime, it has been proposed that relative motion of the radicals forming the pair is inhibited by a relatively rigid microscopic solvent structure.

4.2.2. FT EPR Study of Acetone/2-Propanol

The FT-EPR study[23] of $(CH_3)_2\dot{C}OH$ was concerned with the following topics:

(i) The question of which CIDEP mechanisms play a role. The unequivocal identification of a TM CIDEP contribution is of interest because the effect conveys information on the characteristics—isc spin selectivity, spin-lattice relaxation time—of an excited-state precursor that cannot be studied directly. Particularly intriguing was the possibility of a contribution from a novel CIDEP mechanism.[107]

(ii) The determination of magnitudes of spin polarization. It is difficult to derive magnitudes of spin polarization from TREPR spectra. As pointed out in the Introduction, this is due in part because the time regime over which the time evolution of spectra can be monitored is restricted. The perturbation of the spin system by the microwave field is a complicating factor as well. These factors do not play a role in FT EPR measurements so that one expects to be able to measure the values of spin polarization given by the different CIDEP mechanisms.

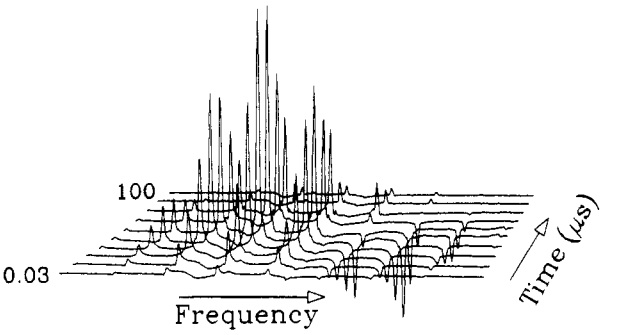

Figure 17. Central portion of the FT EPR spectrum from $(CD_3)_2\dot{C}OD$ in acetone-d_6/2-propanol-d_8 for a series of delay time between laser pulse (308 nm) and microwave pulse. Note that broad lines in the center are due to paramagnetic centers in the quartz dewar insert produced by the UV light. Delay times (from front to back: 0.03, 0.06, 0.10, 0.20, 0.50, 2.0, 5.0, 10, 50, and 100 μs). Reprinted from ref 43; copyright 1988, Weizman Science Press.

(iii) A further objective of the FT EPR investigation was to get information on the kinetics of formation and decay of radical pairs at room temperature. With TREPR it could be shown that radical pairs of $(CH_3)_2\dot{C}OH$ in 2Pr have a lifetime in excess of 1 μs at –80 °C which is attributed to the special solvent characteristics.[106] One would like to be able to study SCRPs at room temperature as well because it may give an insight, at the molecular level, into how solvent molecules affect chemical kinetics. At room temperature the lifetime of SCRPs is too short for them to contribute noticeably to TREPR signals. However, as pointed out in section 3.3, it is possible to probe the characteristics of these transient species with pulsed-EPR methods even under conditions where they may no longer be present at the time the EPR signal is recorded.[58-60]

The FT EPR study[23] of the acetone/2Pr system was mainly concerned with the photochemical reaction of perdeuterioacetone with perdeuterio-2-propanol. Deuterated compounds were employed for two reasons. First, the spectral width of the EPR of the normal acetone ketyl radical far exceeds that covered by the microwave pulse (cf. section 2). FT EPR spectra of this radical show only three of the seven groups of lines (corresponding to a spectral range of ~40 G). Deuteration makes it possible to cover the entire spectral range. Second, the reduction in hyperfine coupling constants by about a factor of 6 removes splittings due to the hydroxyl proton and second-order effects. As a result, $(CD_3)_2\dot{C}OD$ gives a simple 13-line spectrum (hyperfine coupling 2.9 G[55]). TREPR studies[55,104,105] established that EPR spectra of the deuterated radical show CIDEP effects similar to those of the nondeuterated system. Measurements were performed on protonated systems to check for isotope effects on reaction kinetics and spin polarization.

CIDEP Effects, Chemical Kinetics, Relaxation. Figure 17 displays the central portion (70 MHz) of the

FT EPR spectra from $(CD_3)_2\dot{C}OD$ radicals generated by pulsed-laser excitation of acetone-d_6 (1 M) in 2-propanol-d_8 for delays between laser excitation and $\pi/2$ microwave pulse ranging from 30 ns to 100 μs. The spectra are similar to TREPR spectra from $(CD_3)_2\dot{C}OD$[55,104,105] with, for $\tau_d \leq 5$ μs, high-frequency (low-field) peaks in emission and low-frequency peaks in absorption. It is noteworthy that this pattern remains essentially unchanged in the time interval from 30 ns to 5 μs. As pointed out earlier, the rate of triplet spin–lattice relaxation far exceeds the rate of H abstraction. In that case a significant TM CIDEP contribution[102] should grow in with a rate determined by triplet relaxation according to eq 4. Hence, one would expect to see a dominant absorption (or emission) contribution in the spectra obtained with $\tau_d < 100$ ns similar to that found in ZnTPP/DQ and ZnTPP/BQ systems (cf. section 4). At later times, the RPM contribution would gain in relative importance because of diminution of spin polarization in the triplets as they relax to thermal equilibrium. The spectra given in Figure 17 thus point to a small or vanishing TM contribution. This conclusion is confirmed by the quantitative analysis of the evolution of the spectra described below.

Numerical data for the time evolution of the spectral parameters—frequency, amplitude, line width, and phase of seven hyperfine components in the center of the spectrum—were derived with the aid of an LP/SVD-VARPRO analysis[34,35] of the FIDs. A direct analysis of the time dependence of the amplitude of individual hyperfine lines is difficult because it involves a large number of unknowns. However, the data analysis can be simplified by taking advantage of the characteristics of CIDEP contributions. ST_0 RPM CIDEP gives rise to an emission/absorption pattern with inversion symmetry. Spin polarization carried over from precursor triplets gives a contribution in which the relative intensities of hyperfine lines is maintained. Hence, the time evolution of the *difference* in signal amplitudes of $-M$ and $+M$ hyperfine components (ΔS_M) gives the time development of RPM CIDEP. The time evolution of the $M = 0$ signal (S_0) as well as the *sum* of the amplitudes of $+M$ and $-M$ signals ($\sum S_M$) gives the time development of nuclear spin state independent spin polarization contributions such as TM CIDEP.

The time dependence of the ΔS_M, S_0, and $\sum S_M$ signals is shown in Figure 18. The time development of RPM polarization, given in Figure 18a, is governed by the rates of radical formation k_f and spin–lattice relaxation $k_{T_1^R}$. This assumes that the difference signals are dominated by geminate-pair spin polarization contributions. In that case the growth and decay of ΔS_M signals is represented by the following equation:

$$\Delta S_M = \frac{A_M k_f}{k_{T_1^R} - k_f}(e^{-k_f t} - e^{-k_{T_1^R} t}) \qquad (20)$$

The solid lines in Figure 18a represent least-squares fits of the data points to eq 20. The average value of k_f derived from the ΔS_M data is $(6.1 \pm 0.5) \times 10^6$ s^{-1}.

Figure 18 shows that the kinetics of S_0 and $\sum S_M$ signal growth is very similar to that of the ΔS_M signals. A least-squares analysis of the data presented in Figure 18b based on eq 20 gives $k_f = (5.5 \pm 0.4) \times 10^6$ s^{-1}. Evidently, the rate constants derived from the two sets of data do not show a statistically significant difference.

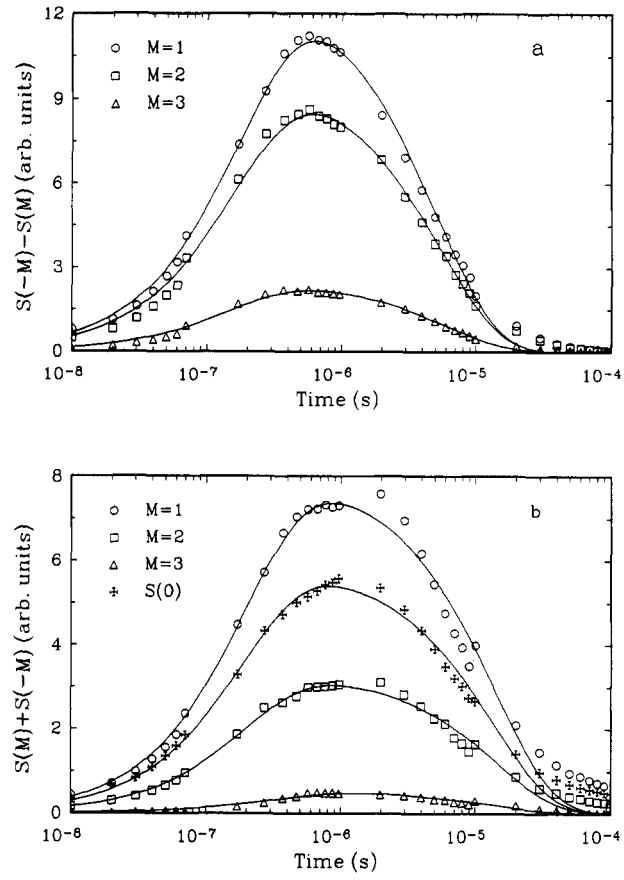

Figure 18. (a) Time dependence of the difference in signal amplitudes of the −1 and +1; −2 and +2; −3 and +3 hyperfine components in the spectrum of $(CD_3)_2\dot{C}OD$. (b) Time dependence of the amplitude of the central hyperfine (S_0) component and the sum ($\sum S_M$) of the +1 and −1; +2 and −2; +3 and −3 hyperfine components. The solid lines give the least-squares fits to the data points based on eq 20. Reprinted from ref 43; copyright 1988; Weizman Science Press.

The result establishes unequivocally that TM CIDEP does not give a noticeable signal contribution.

The data presented in Figure 18 lead to a further, qualitative, conclusion. The least-squares analysis based on eq 20, given by the solid lines in Figure 18, will account satisfactorily for signal decay only if the signal amplitudes reflect strong polarization generated in the radical formation step. In that case, radical decay and associated F-pair spin polarization constitute a small perturbation. As expected, this condition is fulfilled reasonably well for the ΔS_M signals which stem entirely from RPM CIDEP and, for $\tau_d < 10$ μs, are dominated by gemintate-pair spin polarization. The rate of decay of ΔS_M signals, 1.8×10^5 s^{-1}, to a good approximation, represents the ketyl radical spin–lattice relaxation rate so that $T_1^R \approx 5.6$ μs. Equation 20 evidently does not account very well for the decay of the S_0 and $\sum S_M$ signals even in the time domain between 1 and 10 μs (cf. Figure 18b). The inevitable conclusion is that the absorptive signal contribution cannot reflect a strong deviation from thermal equilibrium. The data provide support for the conclusion that the absorptive signal contribution stems from thermalized triplets.[12]

A quantitative analysis of the decay of the S_0 and $\sum S_M$ signal can be given based on a model that considers spin–lattice relaxation ($k_{T_1^R}$) and (second-order) radical decay (k_d). Noting that the EPR experiment measures the time dependence of the population difference

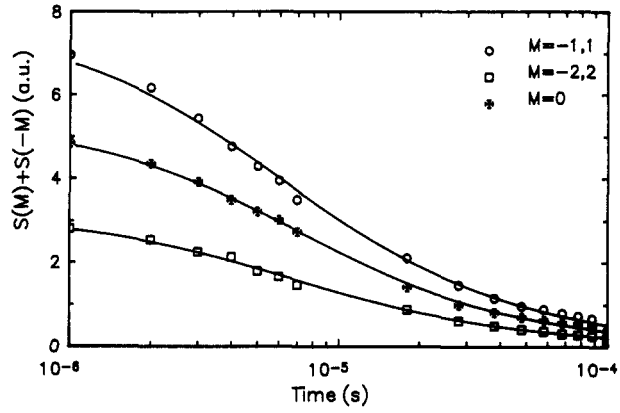

Figure 19. Analysis of the decay of the S_0 and ΣS_m (M = ±1, ±2) signals. The solid lines are least-squares fits to the data points based on eqs 21 and 22. Reprinted from 43; copyright 1988, Weizman Science Press.

between the β and α electron spin states for a given nuclear spin projection M, $\Delta N_M(t) = (N_{\beta_M} - N_{\alpha_M})(t)$, it can be shown that

$$\Delta N_M(t) = P_M(t)N_M(0)[1 + N(0)k_d t]^{-1} \quad (21)$$

where

$$P_M(t) - P_M^{eq} = (P_M(0) - P_M^{eq})e^{-(k_{T_1^R})t} \quad (22)$$

In these equations $P_M(t)$ represents the spin polarization at time t, P_M^{eq} is the Boltzmann spin polarization, $N_M(t)$ gives the number of radicals in nuclear spin state M at time t, and $N(0)$ is the total number of radicals at time zero. Figure 19 shows the results of least-squares fits of the decay of the S_0 and ΣS_M (M = ±1, ±2) signals to eqs 21 and 22. In the analysis τ_d = 2 μs has been taken as time zero. Furthermore, the ratio $P_M(0)/P_M^{eq}$ has been set equal to $^4/_3$ in accordance with the assumption that net absorption originates from thermalized triplets. The average value of the spin–lattice relaxation rate given by the analysis is $k_{T_1^R} = (1.2 \pm 0.3) \times 10^5$ s^{-1}. This gives T_1^R = 8.3 μs as compared to the value of 5.6 μs given by the analysis of the difference signals (vide supra). The relatively large uncertainty in this result is consistent with the presence of a small net absorptive signal contribution. As expected, the rate of chemical decay is determined with a much smaller uncertainty, $k_d N(0) = (1.01 \pm 0.01) \times 10^5$ s^{-1}. The reported second-order rate constant for decay of $(CH_3)_2\dot{C}OH$ is 1×10^9 M^{-1} s^{-1}.[111] From this it can be deduced that a laser flash produces a concentration of ketyl radicals $\approx 10^{-4}$ M. Equations 21 and 22 fail to account satisfactorily for the decay of ΔS_M signals. In this case RPM CIDEP is monitored and it is evident that signal decay is affected by spin polarization generated by chemical decay (F-pair CIDEP).[101]

FT EPR measurements on acetone-h_6/2-propanol-h_8[23] focused on the central three groups of lines representing the M = 0 and M = ±1 hyperfine components. A least-squares analysis of ΔS_1 data based on a first-order signal growth and decay model (eq 20) gave a rate constant of signal growth of 1.1×10^7 s^{-1} and a rate constant of signal decay of $\sim 3.4 \times 10^5$ s^{-1}. Since decay is dominated by spin–lattice relaxation, the measurement gives T_1^R = 2.9 μs in good agreement with published values.[19,106] A comparison of the spectra depicted in Figures 2 and 3 shows that, because of the large difference in hyperfine coupling, ST_0 spin polarization is substantially larger in the spectrum of the protonated radical. For this reason, the decay ΔS_1 will provide a more accurate value for T_1^R.

It has been questioned[107] whether the T_1^R value obtained in the FT EPR study of $(CD_3)_2\dot{C}OD$[23] is correct considering the value for the protonated system. McLauchlan et al. suggest that an analysis of the decay of the S_0 and ΣS_M signals based on T_1^R = 3 μs and leaving the nuclear spin state independent polarization as an adjustable parameter would yield a larger absorptive signal contribution than the one introduced in the original data analysis.[23] A reevaluation[113] of the FT EPR data based on this suggestion confirms that the least-squares procedure is rather insensitive to the choice of the value of T_1^R. However, a lowering of the T_1^R value leads to a reduction in the polarization factor, i.e., it becomes smaller than the value of $^4/_3$ times the Boltzmann polarization used previously. Therefore, the FT EPR data provide no evidence for a CIDEP mechanism that produces net spin polarization in excess of that given by a thermalized triplet precursor.

The time evolution of geminate- and F-pair RPM CIDEP contributions to the FT EPR spectrum from $(CD_3)_2\dot{C}OD$ is given by the ΔS_M difference signals (cf. Figure 18a). Geminate-pair spin polarization will be the dominant contribution to the ΔS_M signals for τ_d < 1 μs since T_1^R and radical decay effects are minimal in this time regime. From the $\Delta S_1/\Sigma_1$, $\Delta S_2/\Sigma_2$, and $\Delta S_3/\Sigma_3$ data, the ratio of the spin polarizations was found to be 1:1.9:2.9. The ratio of ST_0 RPM CIDEP calculated using eqs 5 and 6 (section 3.2) with $\gamma = 0$[48,49] for M ranging from 1 to 6 is 1:1.9:2.6:3.2:3.7:4.1. Clearly there is excellent agreement between experimental and theoretical data for the M = ±1, ±2, ±3 hyperfine components.

For τ_d < 1 μs the magnitude of ΣS_M is a measure of spin polarization carried over from triplets precursors. It was concluded that this polarization amounts to $^4/_3$ times the thermal-equilibrium polarization in doublet radicals (P_{eq}). As long as spin–lattice relaxation and chemical decay do not affect the EPR signal, i.e., for τ_d < 1 μs, the values of the geminate-pair spin polarizations, relative to P_{eq}, are given by $^8/_3(\Delta S_M/\Sigma S_M)$. As expected, the values obtained are constant for 0 ≤ τ_d ≤ 1 μs. For the M = ±1, ±2, ±3 hyperfine components, the geminate polarizations derived from this relationship are 4.2-, 7.9-, and 12.2P_{eq}, respectively. According to eq 5, the magnitude of ST_0 spin polarization is proportional to the square root of the difference in resonance frequency of the radicals making up the pair.[48,49] Taking nuclear spin state degeneracy into account, the relation between ST_0 polarization of the M = 1 hyperfine lines in the spectra of $(CH_3)_2\dot{C}OH$ and $(CD_3)_2\dot{C}OD$ is given by $P_1^H = 1.22(a_H/a_D)^{1/2}P_1^D$. It is assumed here that isotopic substitution does not change the characteristics of the radical pair. The relation gives $P_1^H = 3.18P_1^D$ so that $P_1^H = 13.4P_{eq}$. As expected (cf. section 4.2.1), this value is somewhat lower than the value given by Paul.[12]

Spin-Correlated Radical Pairs. For small τ_d (0–200 ns) the spectra contain a pronounced dispersive signal contribution. This is evident from the delay-time dependence of the signal phase shown in Figure 20 and

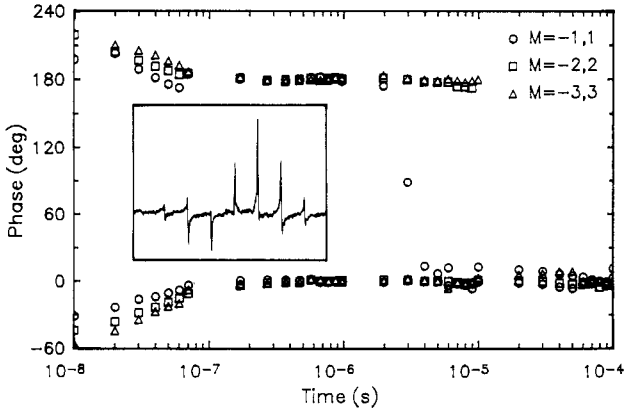

Figure 20. Time evolution of the signal phase of the M = ±1, ±2, ±3 hyperfine components in the spectrum from $(CD_3)_2$·COD. (Note the change from emission (180°) to absorption (0°) of the three high-frequency components in the time region from 3 to 10 μs.) The FT EPR spectrum obtained with τ_d = 10 ns given in the inset shows pronounced dispersive signal contributions. The frequency increases from right to left in this spectrum. Reprinted from ref 43; copyright 1988; Weizman Science Press.

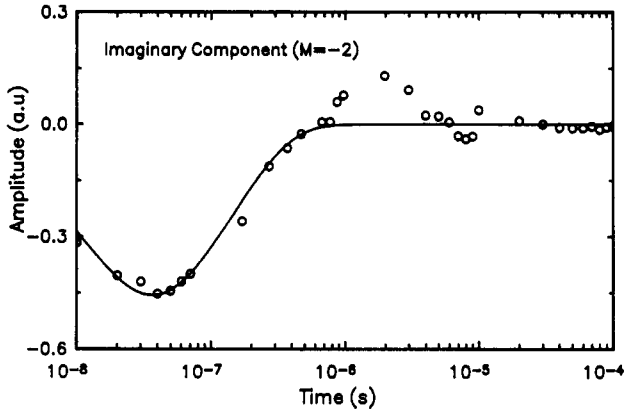

Figure 21. Time dependence of the amplitude of the dispersive component of the M = −2 line in the spectrum from $(CD_3)_2\dot{C}OD$. A least-squares fit of the data points to eq 20 is given by the solid line. Reprinted from ref 43; copyright 1988, Weizman Science Press.

from the line shape of hyperfine components in the FT EPR spectra (cf. inset in Figure 20). As discussed in section 3.3, an out-of-phase signal component is the signature of the presence of SCRPs at the time the $\pi/2$ microwave pulse is delivered.[58-60] It is noted that this signal makes a very minor contribution to the EPR spectrum. For instance, for the ΔM = −2 component, the maximum in the dispersive signal amounts to less than 10% of the maximum in-phase signal amplitude. For τ_d = 1 μs the dispersive signal is less than 2% of the real component.

The time dependence of the amplitude of the dispersive component of the M = −2 signal is displayed in Figure 21. The solid line represents a least-squares fit to the data based on a model that assumes that the paramagnetic species responsible for this signal is formed in a first-order reaction and that its decay is first order as well. Then the time dependence of the amplitude is given by an expression similar to eq 20. Analysis of the time dependence of the out-of-phase signal contributions to six hyperfine components gives an average decay rate constant of (7.5 ± 3.7) × 10^6 s^{-1}. The rate constant of signal growth is ~5 × 10^7 s^{-1}.

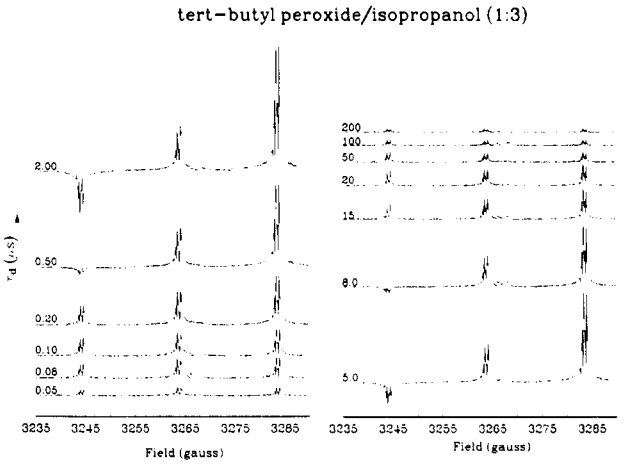

Figure 22. Central portion of the FT EPR spectrum from $(CH_3)_2\dot{C}OH$ produced by photocleavage of *tert*-butyl peroxide in 2-propanol for different delay times between laser and microwave pulses. Signals from the three hyperfine components were measured separately (see section 4.2.3). From ref 108.

4.2.3. FT EPR Study of tert-Butyl Peroxide/2-Propanol

The analysis of the time dependence of the FT EPR spectrum produced by acetone/2Pr is complicated by the fact that both geminate- and F-pair CIDEP contribute to the signal and that, inevitably, spin polarization is transferred from precursor triplets. In the photolysis of *tert*-butyl peroxide (TBP) in 2Pr, ketyl radicals are formed in a reaction of 2Pr with *tert*-butoxy, doublet-spin, radicals according to eq 19. This makes it possible to study the time evolution of F-pair polarization in the absence of geminate pair and TM CIDEP. By removing these sources of spin polarization, the determination of the magnitude of F-pair CIDEP will be easier. Also, the presence of a CIDEP process giving an *enhanced*-absorptive signal contribution[107] will be more readily identified.

Measurements were performed[109] on an Ar-purged solution made up of TBP/2Pr ($^1/_3$ v/v) pumped through an EPR flow cell. The concentration of acetone—generated in radical decay reactions (eqs 17 and 18, section 4.2.1)—was kept small to ensure that it would not affect the results of the study. As noted previously (cf. section 4.2.2), the frequency range covered by the spectrum of $(CH_3)_2\dot{C}OH$ far exceeds the bandwidth of the spectrometer. For this reason the M = −1, 0, and 1 hyperfine lines were measured separately by shifting the magnetic field in order to have the signal of interest on resonance.

Figure 22 shows the central portion of the FT EPR spectrum from $(CH_3)_2\dot{C}OH$ for delay times between laser and microwave pulses ranging from 50 ns to 200 μs. The displayed spectra represent an assemblage of signals given by the central three hyperfine components. The *tert*-butoxy radical cannot be observed because of its short lifetime. For τ_d < 200 ns, the spectra are dominated by an absorptive signal contribution. In the time regime from 100 ns to 50 μs, the effect of F-pair spin polarization is pronounced. F-pair CIDEP turns the M = 1 component into emission over a range of delay times. The low-field emission/high-field absorption pattern corresponds to that found for geminate pair CIDEP.

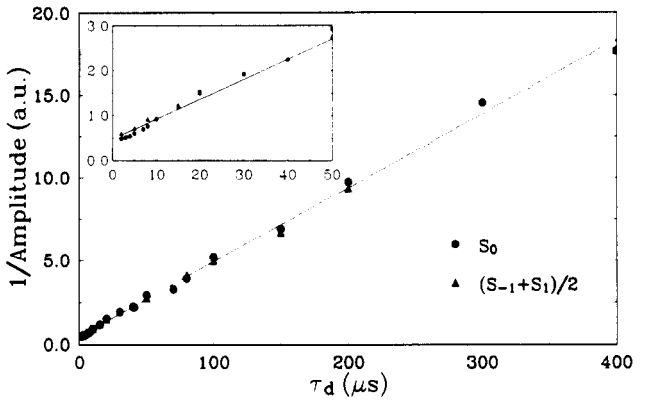

Figure 23. Plot of the inverse of the intensity of the M = 0 peak and average of the M = +1 and −1 peaks versus delay time between laser and microwave pulses. The inset highlights the relationship for 1 μs ≤ τ_d ≤ 50 μs. From ref 108.

To determine if the net-absorption contribution represents spin polarization in excess of the thermal equilibrium value, the decays of the M = 0 peak and the sum of M = 1 and M = −1 peaks (ΣS_1) were analyzed. The time evolution of these signals is not affected by ST_0 CIDEP, but will show the presence of non-Boltzmann, nuclear spin state independent, polarization. Hence, the decays will be determined by second-order chemical decay and, if present, first-order decay of spin polarization. Figure 23 shows that the decays for 2 μs ≤ τ_d ≤ 200 μs closely follow second-order kinetics. From the signal decay and the value for the decay of the acetone ketyl radical in 2Pr ($k_r = 1 \times 10^9$ M^{-1} s^{-1} [11]) it can be calculated that the initial radical concentration is 3.0×10^{-4} M. It follows that the concentration is reduced by about a factor of 2 during the first 3 μs following the laser pulse. Chemical decay at early times accounts for the rapid growing-in of F pair CIDEP that is evident in Figure 22.

No significant systematic deviation from second-order kinetics is observed in the early time regime (see inset in Figure 23). A deviation would be expected if there is a significant enhanced-absorption contribution. In that case spin–lattice relaxation would contribute a first-order decay component. It is concluded that the results provide no evidence for a CIDEP mechanism that gives rise to net enhanced absorption.[107]

The intensities of the M = 0 peak and sum of M = +1 and −1 peaks (ΣS_1 signal) are linearly related to the ketyl radical concentration if only ST_0 F pair CIDEP plays a role and the radicals are formed with *overall Boltzmann* spin polarization. Under those conditions the entire time dependence of the M = 0 and ΣS_1 signals can be described by the rate equation

$$dN^R/dt = k_f N_0^P \exp(-k_f t) - k_d (N^R)^2 \qquad (23)$$

The equation gives the time dependence of the concentration N^R of ketyl radicals with k_f and k_d representing the rate constants of formation and decay, respectively. It is assumed that the *tert*-butoxy radicals—concentration N_0^P—are formed *instantaneously*, that is, within the duration of the laser pulse. It is found that eq 23 does not account for the time evolution of the absorptive signal. Instead, a satisfactory interpretation of the data is obtained with a kinetic model that takes the spin dynamics of the *tert*-butoxy radicals into account. The analysis is based on the

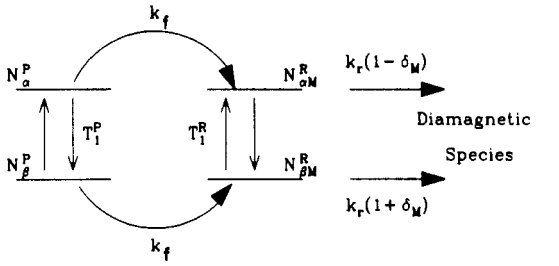

Figure 24. Schematic diagram illustrating the processes that determine the time evolution of the intensities of the hyperfine components in the spectrum of $(CH_3)_2\dot{C}OH$ generated by the reaction of *tert*-butoxy radicals with 2-propanol. For a discussion see text (section 4.2.3). From ref 108.

assumption that the *tert*-butoxy radicals are formed with zero net polarization and that spin–lattice relaxation is slower than, or of the same order of magnitude as, the rate of hydrogen abstraction. A schematic diagram representing the processes that determine the time dependence of the spectrum is shown in Figure 24. According to the model, the population difference ΔN_M^R between β and α spin states for a nuclear spin state M in $(CH_3)_2\dot{C}OH$ is determined by the following:

(i) Spin–lattice relaxation of precursor radicals ($k_{T_1^P}$).

(ii) H abstraction in which spin state is conserved (k_f).

(iii) Spin–lattice relaxation of $(CH_3)_2\dot{C}OH$ ($k_{T_1^R}$).

(iv) Chemical decay in which F pair CIDEP is introduced phenomenologically in the form of a spin-state-dependent reaction rate $k_r(1 \pm \delta_M)$, where the plus and minus signs distinguish decay from β and α electron spin states, respectively, and the subscript M marks the fact that the reaction rate differential δ_M ($|\delta_M| \ll 1$) is a function of nuclear spin state.

The differential equation that represents the time dependence of the Mth hyperfine peak is given by

$$d\Delta N_M^R/dt = k_f f_M P_{eq} N_0^P [e^{-k_f t} - e^{-(2k_{T_1^P}+k_1)t}] - k_d \Delta N_M^R N^R - 2k_{T_1^R} \Delta N_M^R + 2k_{T_1^R} P_{eq} f_M N^R - \delta_M k_d f_M (N^R)^2 \qquad (24)$$

Here f_M represents the nuclear spin state degeneracy, P_{eq} is the Boltzmann spin polarization, N_0^P gives the initial concentration of *tert*-butoxy radicals and N^R the $(CH_3)_2\dot{C}OH$ concentration. δ_M is a, time-independent, F-pair spin polarization factor identical to the parameter used by Paul[12] to account for F-pair polarization in the acetone/2Pr system. For ST_0 CIDEP (pure multiplet effect)

$$\delta_0 = 0, \quad \delta_M = -\delta_{-M}, \quad \sum_M \delta_M N_{M\alpha}^R = -\sum_M \delta_M N_{M\beta}^R$$

Equation 24 was used in a least-squares procedure to describe the intensities of the three central hyperfine peaks in the spectrum of $(CH_3)_2\dot{C}OH$ in the time domain ranging from 10 ns to 400 μs. The analysis made use of previously reported values for T_1^R (2.7 μs[19] and k_d (1×10^9 M^{-1} s^{-1} [111]). The result of the least-squares analysis, executed simultaneously for the three signals, is displayed in Figure 25. The values obtained are $k_f = 2.5 \times 10^7$ s^{-1}, T_1^P = 85 ns, and $|\delta_1| = 3.5 \times P_{eq}$, $N_0^P = 3.8 \times 10^{-4}$ M.

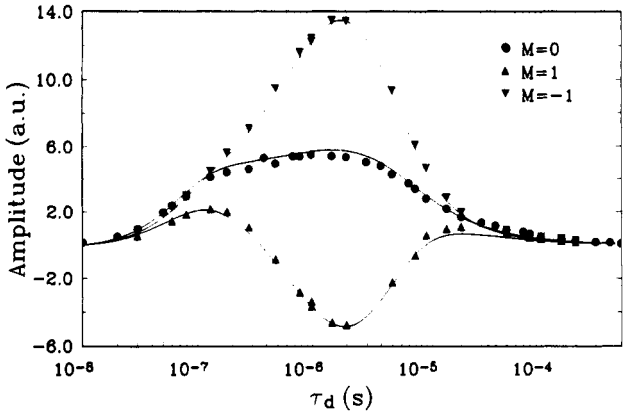

Figure 25. Delay-time dependence of the intensities of the central three hyperfine peaks in the spectrum from $(CH_3)_2\dot{C}OH$ generated by the reaction of *tert*-butoxy radicals with 2-propanol. The solid lines represent the result of a least-squares fit of the data points to eq 24. See text (section 4.2.3) for further details. From ref 108.

4.2.4. Conclusions

First it is of interest to note that the acetone/2-propanol system gives very strong FT EPR signals. As is illustrated in Figures 2 and 3, an FID (data acquisition time 10 μs) generated by a single-laser pulse/microwave-pulse sequence gives spectra with good S/N even for radicals that must be close to thermal equilibrium. This makes it an excellent model system for the development of novel pulsed-EPR techniques for the study of photochemical reactions.

By giving direct information on the time development of the spectra in the first few hundred nanoseconds, the FT EPR spectra could be used to measure: (1) the rate of radical formation for both the acetone/2Pr and TBP/2Pr systems, (2) the magnitude of the spin polarization carried over from paramagnetic precursors-i.e., acetone triplets and *tert*-butoxy doublet radicals, (3) the spin–lattice relaxation time of *tert*-butoxy doublet radicals. The RPM spin-polarization pattern observed establishes that ketyl radical formation in acetone/2Pr involves acetone triplets. On the other hand, the data on TBP/2Pr point to an initial net zero polarization of precursor doublet radicals, a finding that is compatible only with photo-cleavage of singlet excited state TBP.

The magnitudes of the geminate-pair ($13.4P_{eq}$) and F pair ($3.5P_{eq}$) polarization of the $M = \pm 1$ hyperfine peaks show a significant deviation, whereas theory predicts that they should be identical. There are two likely causes for the deviation. First, it should be recalled that the geminate-pair polarization is not measured directly. It is derived from measurements of $(CD_3)_2\dot{C}OD$ by using the theoretically predicted dependence of the polarization on the square root of the hyperfine coupling constant[48,49] (cf. eq 5) in section 3.2). The square-root dependence applies only if the radical pair lifetime remains unchanged. In this system, it is very well possible that a change from deuterated to protonated solvent has an effect on radical pair lifetime. Second, geminate and F pair polarization will have the same value only if singlet-state-forming radical encounters will lead to radical decay with unit probability. For $(CH_3)_2\dot{C}OH$ in propanol this condition is not fulfilled. Apparently, decay from the singlet state has a 0.6 probability only.[114] ST_0 mixing in the radical pairs that are born in the singlet state will generate polarization of opposite sign of that produced by pairs formed in the T_0 state.

FIDs from $(CD_3)_2\dot{C}OD$ in acetone-d_6/2Pr-d_8 for τ_d <200 ns show a pronounced out-of-phase component given by the presence of $[(CD_3)_2\dot{C}OD\cdots(CD_3)_2\dot{C}OD]$ radical pairs in solution. The growth and decay of the signal give the kinetics of formation and decay of this species. At room temperature, the radical pair lifetime is in agreement with a cage-escape rate determined by free diffusive motion of the radicals. By contrast, low-temperature TREPR data provide evidence for "trapping" of the pairs in long-lived solvent cages.[106]

It is noteworthy that ST_0 polarization in the ketyl radical system is appreciably smaller than the values found for ZnTPP/BQ (cf. section 4.1.1). The difference cannot be attributed to a difference in relevant hyperfine interactions. Data on the characteristics of the radical pairs lead to the conclusion that the difference must be due to radical pair lifetimes. At room temperature, the cage-escape rate for the ketyl radicals appears to be determined by free translational diffusion. For $[ZnTPP^+\cdots BQ^-]$, on the other hand, the lifetime is increased appreciably by Coulombic interaction between redox ions.

5. Concluding Remarks

The unique aspect of the application of time-resolved (cw and pulsed) EPR in the study of photochemical reactions is that it can provide a detailed insight into spin-state dynamics of paramagnetic species. Data on relaxation times and CIDEP effects contribute to the understanding of reaction mechanisms and molecular motion. Measurements also can give reliable data on reaction kinetics.

A major advantage of the FT EPR technique is that it considerably simplifies the data analysis compared with that required for spectral data given by time-resolved cw EPR methods. Since the time evolution of spin polarization is not perturbed by a cw microwave field, the spectra more directly reflect spin-state evolution, especially in the early time domain ($0 < \tau_d < 200$ ns). As a consequence, it is easier to identify contributions from different CIDEP mechanisms and gain information on paramagnetic species that do not contribute directly to the spectra. Other advantages include high sensitivity and high spectral resolution.

Given the fact that FT EPR instruments so far have been available only to a few investigators, the accomplishments must be considered very promising. Now that a commercial instrument has become available,[74] one may expect to see a rapid growth of the number of applications, development of novel pulse techniques, and advances in instrumentation. With respect to the last point, it can be noted that improvements in time resolution and bandwidth coverage of the measurements are both desirable and probably not too hard to realize. It will be of special interest to increase the time response to the point that the development of spin polarization in radical pairs can be studied in more detail.

To fully exploit the capabilities of the technique, the methods of data analysis have to be adapted to situations where it is evident that the spin system experiences a significant evolution during the time that the FID is recorded. This is the case, for instance, for

electron transfer in micellar solutions.[45] Spectra from the acetone ketyl radical in 2-propanol also point to an evolution of the system during the first few hundred nanoseconds.[23] Information on radical pair dissociation or movement of radical ions across the boundary between hydrophobic and hydrophilic phases can be contained in the time-domain signal. It will require new data analysis methodologies to take advantage of this fact.

Acknowledgments. H.v.W. owes a debt of gratitude to Dr. Dinse and members of his research group for their kind hospitality and for introducing him to the field of FT EPR applications. Financial support for this work was provided by the Division of Chemical Sciences, Office of Basic Energy Sciences of the U.S. Department of Energy (DE-FG02-84ER-13242), by the Department of Energy University Research Instrumentation Program (DE-FG05-88ER-75441), and by a NATO Collaborative Research Grant.

References

(1) Wertz, J. E. *Chem. Rev.* **1955**, *55*, 829.
(2) Wertz, J. E.; Bolton, J. R. *Electron Spin Resonance: Elementary Theory and Practical Applications*; McGraw-Hill: New York, 1977.
(3) Salikhov, K. M.; Molin, Y. N.; Sagdeev, R. Z.; Buchachenko, A. L. *Spin Polarization and Magnetic Effects in Radical Reactions*; Molin, Y. N., Eds.; Elsevier: Amsterdam, 1984.
(4) Trifunac, A. D.; Lawler, R. G.; Bartels, D. M.; Thurnauer, M. C. *Prog. React. Kinet.* **1986**, *14*, 43.
(5) Hore, P. J. in *Advanced EPR: Applications in biology and biochemistry*; Hoff, A. J., Ed.; Elsevier: Amsterdam, 1989; pp 405–440.
(6) McLauchlan, K. A. In *Modern Pulsed and Continuous-Wave Electron Spin Resonance*; Kevan, L., Bowman, M. K., Eds.; Wiley: New York, 1990; pp 285–364.
(7) Okamura, M. Y.; Feher, G.; Nelson, N. In *Introduction to Photosynthesis: Energy Conversion by Plants and Bacteria*; Govindjee, Ed.; Academic Press: New York, 1982; pp 195–272.
(8) Commoner, B.; Heise, J. J.; Townsend, J. *Proc. Natl. Acad. Sci. U.S.A.* **1956**, *42*, 710.
(9) A critical review of the spectral data is given by: Weaver, E. C. *Annu. Rev. Plant Physiol.* **1968**, *19*, 283.
(10) Norris, J. R.; Uphaus, R. A.; Crespi, H. L.; Katz, J. J. *Proc. Natl. Acad. Sci. U.S.A.* **1971**, *68*, 625.
(11) Smaller, B.; Remko, J. R.; Avery, E. C. *J. Chem. Phys.* **1968**, *48*, 5174.
(12) Paul, H. *Chem. Phys.* **1979**, *40*, 265; **1979**, *43*, 294.
(13) Verma, N. C.; Fessenden, R. W. *J. Chem. Phys.* **1973**, *58*, 2501.
(14) Kim, S. S.; Weissman, S. I. *J. Magn. Reson.* **1976**, *24*, 167.
(15) Forbes, M. D. E.; Peterson, J.; Breivogel, C. S. *Rev. Sci. Instrum.* **1991**, *62*, 2662.
(16) Milov, A. D.; Schirov, M. D.; Khmelinskii, V. E.; Tsvetkov, Y. D. *Dokl. Acad. Nauk SSSR* **1974**, *218*, 878.
(17) Trifunac, A. D.; Norris, J. R. *Chem. Phys. Lett.* **1978**, *59*, 140.
(18) Trifunac, A. D.; Lawler, R. G. *Chem. Phys. Lett.* **1981**, *84*, 515.
(19) Bartels, D. M.; Lawler, R. G.; Trifunac, A. D. *J. Chem. Phys.* **1985**, *83*, 2686.
(20) Dobbert, O.; Prisner, T.; Dinse, K. P. *J. Magn. Reson.* **1986**, *70*, 173.
(21) Massoth, R. J. Thesis, University of Kansas, 1987.
(22) Gorcester, J.; Freed, J. H. *J. Chem. Phys.* **1988**, *88*, 4678.
(23) Levstein, P. R.; van Willigen, H. *J. Chem. Phys.* **1991**, *95*, 900.
(24) Forbes, M. D. E.; Dukes, K. E.; Myers, T. L.; Maynard, H. D.; Breivogel, C. S.; Jaspan, H. B. *J. Phys. Chem.* **1991**, *95*, 10547.
(25) Forbes, M. D. E.; Myers, T. L.; Dukes, K. E.; Maynard, H. D. *J. Am. Chem. Soc.* **1992**, *114*, 353.
(26) Derome, A. *Modern NMR Techniques for Chemistry Research*; Pergamon Press: Oxford, 1987.
(27) Schweiger, A. *Angew. Chem., Int. Ed. Engl.* **1991**, *30*, 265.
(28) Froncisz, W.; Hyde, J. S. *J. Magn. Reson.* **1982**, *47*, 515.
(29) Pfenninger, S.; Forrer, J.; Schweiger, A.; Weiland, Th. *Rev. Sci. Instrum.* **1988**, *59*, 752.
(30) Schweiger, A. In *Modern Pulsed and Continuous-Wave Electron Spin Resonance*; Kevan, L., Bowman, M. K., Eds.; Wiley: New York, 1990; pp 43–118.
(31) Freed, J. H. In *Modern Pulsed and Continuous-Wave Electron Spin Resonance*; Kevan, L., Bowman, M. K., Eds.; Wiley: New York, 1990; pp 119–194.
(32) Prisner, T.; Dobbert, O.; Prisner, T. In *Pulsed EPR: A new field of applications*; Keijzers, C. P., Reijerse, E. J., Schmidt, J., Eds.; North Holland: Amsterdam, 1989; pp 89–95.
(33) Dinse, K. P.; van Willigen, H.; Dobbert, O.; Prisner, T. In *Pulsed EPR: A new field of applications*; Keijzers, C. P., Reijerse, E. J., Schmidt, J., Eds.; Norht Holland: Amsterdam, 1989; pp 89–95.
(34) Barkhuijsen, H.; de Beer, R.; Bouvée, W. M. M. J.; van Ormondt, D. *J. Magn. Reson.* **1985**, *61*, 465.
(35) de Beer, R.; van Ormondt, D. In *Advanced EPR: Applications in biology and biochemistry*; Hoff, A., Ed.; Elsevier: Amsterdam, 1989; pp 135–173.
(36) Wan, J. K. S.; Wong, S. K.; Hutchinson, D. A. *Acc. Chem. Res.* **1974**, *7*, 58.
(37) Adrian, F. J. *J. Chem. Phys.* **1974**, *61*, 4875.
(38) El-Sayed, M. A. *Annu. Rev. Phys. CHem.* **1975**, *26*, 235.
(39) van der Waals, J. H.; van Dorp, W. G.; Schaafsma, T. J. In *The Porphyrins*; Dolphin, D., Ed.; Academic Press: New York, 1979; Vol. 4, pp 257–312.
(40) Atkins, P. W.; Evans, G. T. *Mol. Phys.* **1974**, *27*, 1633.
(41) Atkins, P. W.; Dobbs, A. J.; McLauchlan, K. A. *Chem. Phys. Lett.* **1974**, *29*, 616.
(42) Basu, S.; Grant, A. I.; McLauchlan, K. A. *Chem. Phys. Lett.* **1983**, *94*, 517.
(43) Bowman, M. K.; Toporowicz, M.; Norris, J. R.; Michalski, T. J.; Angerhofer, A.; Levanon, H. *Isr. J. Chem.* **1988**, *28*, 215.
(44) Angerhofer, A.; Toporowicz, M.; Bowman, M. K.; Norris, J. R.; Levanon, H. *J. Phys. Chem.* **1988**, *92*, 7164.
(45) Levstein, P. R.; van Willigen, H. *Chem. Phys. Lett.* **1991**, *187*, 415.
(46) Leinwand, D. A.; Lefkowitz, S. M.; Brenner, H. C. *J. Am. Chem. Soc.* **1985**, *107*, 6179.
(47) Kaptein, R.; Oosterhoff, L. J. *Chem. Phys. Lett.* **1969**, *4*, 214.
(48) Adrian, F. J. *J. Chem. Phys.* **1971**, *54*, 3918.
(49) Freed, J. H.; Pedersen, J. B. *Adv. Magn. Res.* **1976**, *8*, 1.
(50) Trifunac, A. D. *Chem. Phys. Lett.* **1977**, *49*, 457.
(51) Trifunac, A. D.; Nelson, D. J. *Chem. Phys. Lett.* **1977**, *46*, 346.
(52) Burkey, T. J.; Lusztyk, J.; Ingold, K. U.; Wan, J. K. S.; Adrian, F. J. *J. Phys. Chem.* **1985**, *89*, 4286.
(53) Buckley, C. D.; Hunter, D. A.; Hore, P. J.; McLauchlan, K. A. *Chem. Phys. Lett.* **1987**, *135*, 307.
(54) Closs, G. L.; Forbes, M. D. E.; Norris, J. R. *J. Phys. Chem.* **1987**, *91*, 3592.
(55) Tominaga, K.; Yamauchi, S.; Hirota, N. *Chem. Phys. Lett.* **1988**, *149*, 32.
(56) Stehlik, D.; Bock, C. H.; Petersen, J. *J. Phys. Chem.* **1989**, *93*, 1612.
(57) Hasharoni, K.; Levanon, H.; Tang, J.; Bowman, M. K.; Norris, J. R.; Gust, D.; Moore, T. A.; Moore, A. L. *J. Am. Chem. Soc.* **1990**, *112*, 6477.
(58) Thurnauer, M. C.; Norris, J. R. *Chem. Phys. Lett.* **1980**, *76*, 557.
(59) Dinse, K. P.; Plüschau, M.; Kroll, G.; Prisner, T.; van Willigen, H. *Bull. Magn. Reson.* **1989**, *11*, 174.
(60) Kroll, G.; Plüschau, M.; Dinse, K. P.; van Willigen, H. *J. Chem. Phys.* **1990**, *93*, 8709.
(61) Imamura, T.; Onitsuka, O.; Obi, K. *J. Phys. Chem.* **1986**, *90*, 6741.
(62) Jenks, W. S.; Turro, N. J. *Tetrahedron Lett.* **1989**, *30*, 4469.
(63) Blättler, C.; Jent, F.; Paul, H. *Chem. Phys. Lett.* **1990**, *166*, 375.
(64) Kawai, A.; Okutsu, T.; Obi, K. *J. Phys. Chem.* **1991**, *95*, 9130.
(65) Kawai, A.; Obi, K. *J. Phys. Chem.* **1992**, *96*, 52.
(66) van Willigen, H.; Levstein, P. R., 1991, unpublished results.
(67) Plüschau, M.; Zahl, A.; Dinse, K. P.; van Willigen, H. *J. Chem. Phys.* **1989**, *90*, 3153.
(68) Ebersole, M.; Levstein, P. R.; van Willigen, H. *J. Phys. Chem.*, in press.
(69) Ebersole, M. Thesis, University of Massachusetts, 1992.
(70) Levstein, P. R.; van Willigen, H.; Ebersole, M. H.; Pijpers, F. W. *Mol. Cryst. Liq. Cryst.* **1991**, *194*, 123.
(71) Levstein, P. R.; van Willigen, H., to be published.
(72) Berman, A.; Michaeli, A.; Feitelson, J.; Bowman, M. K.; Norris, J. R.; Levanon, H.; Vogel, E.; Koch, P. *J. Phys. Chem.* **1992**, *96*, 3041.
(73) Beckert, D.; Plüschau, M.; Dinse, K. P. *J. Phys. Chem.* **1992**, *96*, 3193.
(74) Zilber, G.; Rozenshtein, V.; Rabinovitz, M.; Levanon, H. *Chem. Phys. Lett.*, in press.
(75) Venkataraman, B.; Segal, B. G.; Fraenkel, G. K. *J. Chem. Phys.* **1959**, *30*, 1006.
(76) Hoffman, B. *J. Am. Chem. Soc.* **1975**, *97*, 1688.
(77) Chan, I. Y.; van Dorp, W. G.; Schaafsma, T. J.; van der Waals, J. H. *Mol. Phys.* **1971**, *22*, 741, 753.
(78) Shushin, A. I. *Chem. Phys. Lett.* **1989**, *162*, 409.
(79) Ware, W. R.; Novros, J. S. *J. Phys. Chem.* **1966**, *70*, 3246.
(80) Nemzek, T. L.; Ware, W. R. *J. Chem. Phys.* **1975**, *62*, 477.
(81) Stevens, B. *Chem. Phys. Lett.* **1987**, *134*, 519.
(82) Stevens, B.; McKeithan, D. N. *J. Photochem. Photobiol. A* **1987**, *40*, 1.
(83) Smoluchowski, M. V. *Z. Phys. Chem.* **1917**, *92*, 129.
(84) Harriman, A.; Porter, G.; Searle, N. *J. Chem. Soc., Faraday Trans.* **1979**, *279*, 1515.
(85) Pileni, M. *Chem. Phys. Lett.* **1980**, *75*, 540.
(86) Schlüpmann, J.; Salikhov, K. M.; Plato, M.; Jaegerman, P.; Lendzian, F.; Möbius, K. *Appl. Magn. Reson.* **1991**, *2*, 117.

(87) van Willigen, H.; Vuolle, M.; Dinse, K. P. *J. Phys. Chem.* **1989**, *93*, 2441.
(88) Pople, J. A.; Schneider, W. G.; Bernstein, H. J. *High Resolution Nuclear Magnetic Resonance*; McGraw-Hill: New York, 1959.
(89) Angerhofer, A.; Massoth, R. J.; Bowman, M. K. *Isr. J. Chem.* **1988**, *28*, 227.
(90) Kalyanasundaram, K. *Photochemistry in microheterogeneous systems*; Academic Press: New York, 1987.
(91) Grätzel, M. In *Supramolecular photochemistry*; Balzani, V., Ed.; NATO ASI Series; Reidel: Dordrecht, 1987; p 435.
(92) Kadish, K. M.; Maiya, G. B.; Araullo, C.; Guillard, R. *Inorg. Chem.* **1989**, *28*, 2725.
(93) Leniart, D. S.; Connor, H. D.; Freed, J. *J. Chem. Phys.* **1975**, *63*, 165.
(94) Suga, K.; Maemura, K.; Fujihira, M.; Aoyagui, S. *Bull. Chem. Soc. Jpn.* **1987**, *60*, 2221.
(95) Johnston, L. J. In *Photochemistry in Organized and Constrained Media*; Ramamurthy, V., Ed.; VCH Publishers: New York, 1991; pp 359–386.
(96) Levstein, P. R.; van Willigen, H., to be published.
(97) Kazanis, S.; Azarani, A.; Johnston, L. J. *J. Phys. Chem.* **1991**, *95*, 4430.
(98) Livingston, R.; Zeldes, H. *J. Chem. Phys.* **1966**, *44*, 1245.
(99) Wong, S. K.; Chiu, T.-M.; Bolton, J. R. *J. Phys. Chem.* **1981**, *85*, 12.
(100) Grant, A. I.; Grenn, N. J. B.; Hore, P. J.; McLauchlan, K. A. *Chem. Phys. Lett.* **1984**, *110*, 280.
(101) Thurnauer, M. C.; Chiu, T.-M.; Trifunac, A. D. *Chem. Phys. Lett.* **1985**, *116*, 543.
(102) Yamauchi, S.; Tominaga, K.; Hirota, N. *J. Phys. Chem.* **1986**, *90*, 2367.
(103) Buckley, C. D.; McLauchlan, K. A. *Chem. Phys. Lett.* **1987**, *137*, 86.
(104) Tominaga, K.; Yamauchi, S.; Hirota, N. *J. Chem. Phys.* **1988**, *88*, 553.
(105) Tominaga, K.; Yamauchi, S.; Hirota, N. *J. Phys. Chem.* **1988**, *92*, 5160.
(106) Tominaga, K.; Yamauchi, S.; Hirota, N. *J. Chem. Phys.* **1990**, *92*, 5175.
(107) McLauchlan, K. A.; Simpson, N. J. K.; Smith, P. D. *Res. Chem. Intermed.* **1991**, *16*, 141.
(108) Shkrob, I. A.; Wan, J. K. S. *Res. Chem. Intermed.* **1992**, *17*, 77.
(109) Levstein, P. R.; Doering, P.; van Willigen, H. *Chem. Phys. Lett.*, submitted for publication.
(110) Porter, G.; Dogra, S. K.; Loutfy, R. O.; Sugamori, S. E.; Yip, R. W. *J. Chem. Soc., Faraday Trans.* **1973**, *1*, 1462.
(111) Lehni, M.; Fischer, H. *Int. J. Chem. Kinet.* **1983**, *15*, 733.
(112) Yamauchi, S.; Tominaga, K.; Hirota, N. *Abstr. 5th Nodzu Memorial Lectures* **1985**, 24.
(113) Levstein, P. R., unpublished results.
(114) Münger, K.; Fischer, H. *Int. J. Chem. Kinet.* **1984**, *16*, 1213.